Naval Surface Warfare Center
Carderock Division
West Bethesda, MD 20817-5700

NSWCCD-70-TR–2004/058 May 2004

Signatures Directorate

Technical Report

A Criterion for Conversion of Summations to Integrations in Structural Acoustics

by

G. Maidanik

K. J. Becker

L. J. Maga

[Work supported by ONR and In-House Fundings.]

NSWCCD-70-TR—2004/058 May 2004 A Criterion for Conversion of Summations to Integrations in Structural Acoustics

Naval Surface Warfare Center
Carderock Division

NSWCCD-70-TR–2004/058 May 2004

Signatures Directorate

Technical Report

West Bethesda, MD 20817-5700

A Criterion for Conversion of Summations to Integrations in Structural Acoustics

by

G. Maidanik

K. J. Becker

L. J. Maga

[Work supported by ONR and In-House Fundings]

REPORT DOCUMENTATION PAGE

Form Approved
OMB No. 0704-0188

1. REPORT DATE *(DD-MM-YYYY)*	2. REPORT TYPE	3. DATES COVERED *(From - To)*
1-May-2004	Final	-

4. TITLE AND SUBTITLE

A Criterion for Conversion of Summations to Integrations in Structural Acoustics

5a. CONTRACT NUMBER

5b. GRANT NUMBER

5c. PROGRAM ELEMENT NUMBER

6. AUTHOR(S)

G. Maidanik, K. J. Becker and L. J. Maga

5d. PROJECT NUMBER

5e. TASK NUMBER

5f. WORK UNIT NUMBER

7. PERFORMING ORGANIZATION NAME(S) AND ADDRESS(ES) AND ADDRESS(ES)

Naval Surface Warfare Center
Carderock Division
9500 Macarthur Boulevard
West Bethesda, MD 20817-5700

8. PERFORMING ORGANIZATION REPORT NUMBER

NSWCCD-70-TR-2003/058 May 2004

9. SPONSORING / MONITORING AGENCY NAME(S) AND ADDRESS(ES)

Attn ONR 334
Chief of Naval Research
Ballston Centre Tower One
800 North Quincy Street
Arlington, VA 22217-5660

10. SPONSOR/MONITOR'S ACRONYM(S)

11. SPONSOR/MONITOR'S REPORT NUMBER(S)

12. DISTRIBUTION / AVAILABILITY STATEMENT

Approved for public release; distribution is unlimited.

13. SUPPLEMENTARY NOTES

14. ABSTRACT

An analytical formulation of a transfer function pertaining to a simple structural model is used to examine this criterion. The model consists of a coated plate immersed in fluid media on either side. The first fluid interfaces the coating atop and is semi-infinite in extent. The second fluid interfaces the bottom of the plate and terminates at a baffle that defines a reflection coefficient. An external drive is placed on a plane that lies in the fluid between the plate and the baffle. Focus is centered on the transfer function of a spectral component in the external drive to a spectral component on the inter-face with the top fluid. The presence of the baffle generates, in this transfer function, resonances and anti-resonances. These are discernible in those regions of the frequency domain in which the modal overlap parameters are less than unity. In those regions of the frequency domain in which the modal overlap parameters exceed unity the resonances and the anti-resonances merge onto values that are conditioned by the absence of the cavity. It transpires that converting a summation to an integration is tantamount to merging artificially the resonances and the anti-resonances also in those regions in which the modal overlap parameters are less than unity. The merging, again, are onto values that are conditioned by the absence of the cavity.

15. SUBJECT TERMS

16. SECURITY CLASSIFICATION OF:			17. LIMITATION OF ABSTRACT	18. NUMBER OF PAGES	19a. NAME OF RESPONSIBLE PERSON
a. REPORT	b. ABSTRACT	c. THIS PAGE			G. Maidanik
UNCLASSIFIED	UNCLASSIFIED	UNCLASSIFIED	UL	68	19b. TELEPHONE NUMBER *(include area code)* 301-227-1292

Contents

A Criterion for Conversion of Summations to Integrations in Structural Acoustics

G. Maidanik, K. J. Becker and L. J. Maga

Abstract

An analytical formulation of a transfer function pertaining to a simple structural model is used to examine this criterion. The model consists of a coated plate immersed in fluid media on either side. The first fluid interfaces the coating atop and is semi-infinite in extent. The second fluid interfaces the bottom of the plate and terminates at a baffle that defines a reflection coefficient. An external drive is placed on a plane that lies in the fluid between the plate and the baffle. Focus is centered on the transfer function of a spectral component in the external drive to a spectral component on the interface with the top fluid. The presence of the baffle generates, in this transfer function, resonances and anti-resonances. These are discernible in those regions of the frequency domain in which the modal overlap parameters are less than unity. In those regions of the frequency domain in which the modal overlap parameters exceed unity the resonances and the anti-resonances merge onto values that are conditioned by the absence of the

cavity. It transpires that converting a summation to an integration is tantamount to merging artificially the resonances and the anti-resonances also in those regions in which the modal overlap parameters are less than unity. The merging, again, are onto values that are conditioned by the absence of the cavity. It follows then that in those regions of the frequency domain, where resonances and anti-resonances roam under summations, converted to integrations, these resonances and anti-resonances are, thereby, suppressed.

I. Introduction

Why does SEA (statistical energy analysis) exceed expectation even though its validity is not always on hand? In SEA, by its very definition, energy is conserved. The "conservation of energy" is a law of nature that stood the passage of time, also without its validity on hand. The "statistical" in SEA is meant to simplify the analysis and the computations thereof, but it also smoothes out details. The estimates that are issued by SEA are usually smoother than those issued by EA (energy analysis) and/or by measured data. [For example, the tenet in SEA of equi-partition of modal energies in the modes of a given dynamic system renders the sum over modes simple. Simultaneously this tenet suppresses the modal variability in the estimated response [1].] Thus, a gross agreement, between estimates issued by SEA and the *averaged* measured data, may be deemed adequate. Disagreement in the details is not considered to be a disagreement in the estimates provided by SEA and the measured data. Some examination of the validity of SEA, vis-à-vis details in the data, are to be answered by higher statistics [2-7]. These higher statistics need be applied to both, to the measured data and to the estimates that embody details that are a priori smoothed out by SEA. There have been attempts afoot to introduce these higher

statistics [1, 2-7]. Although some of these attempts have been crowned successful; our best wishes still go to those so engaged. This remark forewarns that this report is not concerned with these higher statistics.

This report largely deals with one of two topics that bear on the remark just made. The first of these two relates to the fundamental question whether the estimates of the *power input* into a complex dynamic system is adequately accounted for in SEA [1, 2 and 8-12]. Often, the (steady state) power input into the *driven* dynamic system is estimated, in SEA, on the basis that the power is independent of the couplings of this dynamic system to the others in the complex. An estimate of this kind usually tends to underestimate the power input. This underestimate results in an overestimation of the noise control effectiveness of the couplings to those other dynamic systems in the complex. This overestimate of the noise control effectiveness of the couplings negates Le Chatelier's Principle [12, 13]. The second topic relates to the conditions that need to be met by the complex dynamic system when summations may be legitimately converted to integrations [14-19]. This criterion has a great deal to do with the availability and the significance of the higher statistics in the estimates of SEA as just mentioned. It is this second topic that is touched upon in this report.

"Touched upon" rather than "considered" because the topic is merely and briefly illustrated rather than delved into and analyzed in detail. The complex dynamic system of choice is a *plane and a plain* resonating structure immersed in fluids on either side of the structure, and the response of choice is cast in terms of a specific *transfer function*.

In Section II the complex dynamic system, selected for the study of the transfer functions in which *resonances* and *anti-resonances* are manifested, is described and defined. The formalism is focused on the transfer function that governs the transfer of spectral components in the external drive to spectral components that emerge on the interface of a coated plate with the top fluid. [cf. Figure 1.] The top fluid occupies the semi-infinite space above that interface. The external drive is placed on a plane parallel to the plate in the bottom fluid a specific normalized distance below the plate. Since there are no discontinuities, either in the plate or in the coating and these elements of the structure are assumed to be isotropic, the transfer is one-to-one; a spectral component in the external drive is spectrally duplicated in the component that emerges on the interface with the top fluid. The spectral component that is selected for investigation in this report is supersonic. To render, in this transfer function, resonances

(amplifications) and anti-resonances (attenuations) a baffle is placed in the bottom fluid on a parallel plane to the plate. The baffle is uniform and it lies below the plane in which the external drive resides. Assisted by Figure 1, the analytical expressions for the transfer function are derived. The transfer function (T_{bc}), in the presence of the cavity and of the coating, is derived first. The presence of the cavity is designated by the subscript (b) and that of the coating by the subscript (c). The reductions in the expression for the transfer function (T_{bc}) to (T_c), when the cavity is removed, to (T_b), when the coating is removed, and to (T), when the cavity as well as the coating are removed, are derived successively.

In Section III computations pertaining to the transfer functions (T_{bc}), (T_c), (T_b) and (T), as functions of an appropriately normalized frequency, are carried out. As expected, resonances and anti-resonances are found only in the results of computations involving (T_{bc}) and (T_b). After all, these are the only transfer functions governed by the presence of the cavity. In the absence of the cavity the resonances and the anti-resonances are absent. The results of computations involving (T_c) and (T) are, indeed, devoid of resonances and

anti-resonances. The results of the computations are presented graphically in a set of three graphs. In the first graph the modulus of (T_{bc}) is depicted by a solid curve and the modulus of (T_c) is depicted by a dotted curve. In the second graph the modulus of (T_b) is depicted by a solid curve and the modulus of (T) is depicted by a dotted curve. Each of these two graphs contrast the transfer function in the presence of the cavity (solid curves) with the corresponding transfer function in the absence of the cavity (dotted curves). In the third graph the modulus of (T_{bc}/T_b) is depicted by a solid curve and the modules of (T_c/T) is depicted by a dotted curve. This third graph exhibits and contrasts the influence of the coating on the transfer function in the presence of the cavity (solid curve) with the transfer function in the absence of the cavity (dotted curve). The influence on the transfer functions of *damping* in the cavity is also computed and investigated. Both, the volume (bulk) damping and the damping resulting from the absorption in the surface of the baffle, are considered. The role played by the *modal overlap parameter* is of particular investigative and interpretive interest. Modal overlap parameters that exceed unity suppress the presence of resonances and anti-resonances in the transfer functions. The convergence of the peaks in the

resonances and the nadirs in the anti-resonances onto the dotted curves that depict the transfer functions in the absence of the cavity is also of particular interest in this report. The convergence is complete only in those regions of the normalized frequency in which the modal overlap parameters exceed unity. In those regions in which the modal overlap parameters are less than unity resonances and anti-resonances prevail.

In Section IV summations in the expressions for the transfer functions, under several varying conditions of damping, are converted to corresponding integrations. The results of computations, carried out under judicious evaluations, show that the resonances and the anti-resonances, that exist when the summations prevail, are suppressed when these summations are converted to the corresponding integrations. It is interpreted that in those regions of the frequency domain in which the modal overlap parameters are less than unity, the conversion of the summations to integrations is tantamount to inducing artificially these modal overlap parameters to exceed unity. One recalls that in a region where the modal overlap parameters are less than unity, the footprints of the resonances and the anti-resonances are clearly discernible. Thus, the conversion of the summations to the corresponding integrations suppresses the modal character of the transfer functions here investigated.

The suppression is such as to validate the "mean-value method" proposed by Skudrzyk [20].

Finally, a number of variations on the theme are covered in an Appendix. These are presented under a separate cover in order not to clutter the main theme of the paper. That theme is to decipher the meanings and the procedures that encompass the conversion of summations to integrations in structural acoustics. It is hoped that this limited theme is adequately illustrated and that the arguments are convincing enough. (Beware, if we failed, you will have to read another paper by us on the same subject. Could this be more threatening?!)

II. Derivation of the expressions for the transfer function

The illustration is conducted on the dynamic system shown in Figure 1. This dynamic system is composed basically of a plate immersed, on each side, by a fluid; fluid no. 1 atop and fluid no. 2 below. The plate is backed by a baffle. The baffle is uniform and is placed on a plane a normalized distance (b) below the plate; $b = (b_1 + b_2)$. The normalizing factor is the wavenumber (ω_o / c_1), where (ω_o) is a specific frequency and (c_1) is the speed of sound in the top fluid (fluid no. 1). A thin slab of compliant coating is attached to the top side of the plate, the other side of the coating interfaces the fluid atop (fluid no. 1) as depicted in Figures 1a and 1b. The surface stiffness (K_c) of the coating forms with the surface mass (m) of the plate an oscillator which resonance frequency is (ω_o), given by $(\omega_o)^2 = (K_c / m)$. In this report (ω_o) is used, except for self, as a normalizing factor for all frequencies and time scales. Similarly, as already stated, all wavenumbers and spatial scales are here normalized by (ω_o / c_1). A set of external drives are distributed on a plane a normalized distance (b_1) below the plane of the plate as indicated in Figure 1a. It is conditioned that

$(b_1) < (b)$. The transfer function $T_{bc}(\mathbf{k},\omega)$, relating the spectral component $P_e(\mathbf{k},\omega)$, in the external drive, to the spectral component $P_{f1}(\mathbf{k},\omega)$, in the pressure on the interface with the semi-infinite fluid atop (fluid no. 1), is of special interest in this report. The subscript (b) in (T_{bc}) designates the presence of the cavity and the subscript (c) designates the presence of the coating. The normalized vector $\{\mathbf{k},\omega\}$ is a spectral variable, where $(\mathbf{k})$ is the normalized wavevector in the plane of the plate and (ω) is the normalized frequency. The normalizing factors, once again, are the wavenumber (ω_o/c_1) and the frequency (ω_o), respectively. The analytical derivation of this transfer function is assisted by Figure 1. In particular, by Figure 1c and by the synopsis of the analysis given in Figure 1d. In this vein one defines and derives the transfer function $T_{bc}(\mathbf{k},\omega)$ in the form

$$T_{bc}(\mathbf{k},\omega)=[P_{f1}(\mathbf{k},\omega)/P_e(\mathbf{k},\omega)] \quad ; \quad P_{f1}(\mathbf{k},\omega)=[Z_{f1}(\mathbf{k},\omega)V_1(\mathbf{k},\omega)] \quad ;$$

$$T_{bc}(\mathbf{k},\omega) = Z(\mathbf{k},\omega)G(\mathbf{k},\omega)C(\mathbf{k},\omega) \quad , \text{(1a)}$$

where $V_1(\mathbf{k},\omega)$ is the response of the interface of the coating with fluid no. 1, $Z(\mathbf{k},\omega)$ is a parallel combination of the fluid surface impedance $Z_{f1}(\mathbf{k},\omega)$ and the surface (stiffness) impedance $Z_c(\mathbf{k},\omega)$ of the coating; namely

$$Z(\mathbf{k},\omega) = Z_{f1}(\mathbf{k},\omega)Z_c(\mathbf{k},\omega)[Z_{f1}(\mathbf{k},\omega) + Z_c(\mathbf{k},\omega)]^{-1} \quad , (2)$$

and $G(\mathbf{k},\omega)$ is the surface admittance of the plate in situ

$$G(\mathbf{k},\omega) = [Z(\mathbf{k},\omega) + Z_p(\mathbf{k},\omega) + Z^b_{f2}(\mathbf{k},\omega)]^{-1} \quad . (3)$$

In Equations (1a), (2) and (3) the surface impedances are all normalized. The normalizing factor here is the imaginary part of the surface mass impedance; i.e., $[(m\omega_o)(\omega)]$, of the plate. Thus, for example, the normalization of the surface impedance of the coating is

$$Z_c(\mathbf{k},\omega) = Z_c(\omega) = -i[K_c(1+i\eta_c)/(m\omega_o^2)(\omega)^2] = -i(\omega)^{-2}(1+i\eta_c) \quad ;$$

$$\omega_o^2 = (K_c/m) \quad , (4)$$

and the normalization of the surface impedance of the top fluid (fluid no. 1) is

$$Z_{f1}(\mathbf{k},\omega) = Z_{f1}(k,\omega) = \gamma_1(\omega_c/\omega)[k_{31}(k,\omega)]^{-1} \quad ; \quad \gamma_1 = (\rho_1 c_1/\omega_o \omega_c m) \quad ;$$

$$k_{31}(k,\omega) = (1-\alpha_1^2)^{1/2}\, U(1-\alpha_1^2) - i(\alpha_1^2-1)^{1/2}\, U(\alpha_1^2-1) \quad ;$$

$$\alpha_1^2 = (k/\omega)^2 \quad ; \quad |\mathbf{k}| = k \qquad , (5a)$$

where (U) is the standard step function, $(\rho_1 c_1)$ is the characteristic impedance of fluid no. 1 and (ω_c) is the normalized critical frequency of the plate with respect to the top fluid (fluid no. 1). Again, the normalizing factor for the critical frequency is (ω_o). In this report K_c is simply assumed to be a constant independent of $(\mathbf{k})$ and (ω). The normalized wavenumber $k_{31}(k,\omega)$ is the *viable* wavenumber in the top fluid (fluid no. 1) that describes, in that fluid, the propagation normal to the plane of the plate. As indicated in Equation (5a) this wavenumber is dependent merely on (k) not on $(\mathbf{k})$ and, therefore, so is the normalized surface fluid impedance. The normalized fluid loading on the plate, due to the bottom fluid (fluid no. 2), is modified by the presence of the cavity in the manner

$$Z^b_{f2}(\mathbf{k},\omega) = Z^b_{f2}(k,\omega) = A(k,\omega)\,Z_{f2}(k,\omega) \qquad , (6)$$

where $Z_{f2}(k,\omega)$ is the normalized surface impedance of the bottom fluid in the absence of the cavity; namely

$$Z_{f2}(\mathbf{k},\omega) = Z_{f2}(k,\omega) = \gamma_2(\omega_c/\omega)[k_{32}(k,\omega)]^{-1} \quad ; \quad \gamma_2 = (\rho_2 c_2/\omega_o \omega_c m) \quad ;$$

$$k_{32}(k,\omega) = (1-\alpha_2^2)^{1/2}\, U(1-\alpha_2^2) - i(\alpha_2^2-1)^{1/2}\, U(\alpha_2^2-1) \quad ;$$

$$\alpha_2^2 = (c_2/c_1)^2\alpha_1^2 \quad ; \quad |\mathbf{k}| = k \qquad , (5b)$$

In Equation (5b) $(\rho_2 c_2)$ is the characteristic impedance of fluid no. 2 and $k_{32}(k,\omega)$ is the normalized viable wavenumber that describes the propagation normal to the plane of the plate in the bottom fluid (fluid no. 2). [cf. Equation (5b).] The dimensionless factor $A(k,\omega)$ accounts for the modification, by the presence of the cavity, to the surface impedance of the bottom fluid (fluid no. 2). The expression for this factor may be derived by tracing the multiple reflections at the blocked plate and the surface of the cavity. The result is

$$Z^{b}_{f2}(k,\omega) = Z_{f2}(k,\omega)\,A(k,\omega) \quad ; \quad A(\mathbf{k},\omega) = A(k,\omega) \quad ;$$

$$A(k,\omega) = [1 + R(\omega)\exp\{\mathrm{a}(k,\omega)\}]\,[1 - R(\omega)\exp\{\mathrm{a}(k,\omega)\}]^{-1} \quad ;$$

$$\mathrm{a}(k,\omega) = \{-2i(c_1/c_2)(b\omega)\,k_{32}(k,\omega)\}(1 - i\eta) \quad , (7a)$$

where (η) is the volume loss factor in the cavity, $\mathrm{a}(k,\omega)$ is the argument of the propagator in the bottom fluid form the plane of the plate to the surface of the baffle and back again, and $R(\omega)$ is the reflection coefficient on the surface of this baffle. Again, the reflection coefficient is here assumed, for simplicity sake, to be independent of the wavevector $(\mathbf{k})$. There remains to define just another dimensionless factor; the $C(k,\omega)$ in Equation (1). This dimensionless factor accounts for the modification to the external drive by the presence of the cavity. This factor adjusts for any off-set, of the external drive, from the plane of the cavity before the multiple reflections in the cavity commence. This factor may be expressed in the form

$$P^{b}_{e}(\mathbf{k},\omega) = C(k,\omega)P_{e}(\mathbf{k},\omega) \quad ;$$

$$C(k,\omega) = [1 + (-1)^{s} R(\omega)\,\exp\{\mathrm{as}(k,\omega)\}]\,[1 - R(\omega)\exp\{\mathrm{a}(k,\omega)\}]^{-1} \quad ;$$

$$\mathrm{as}(k,\omega) = \{-2i(c_1/c_2)[\omega(b - b_1)]\,k_{32}(k,\omega)\}(1 - i\eta) \quad , (7b)$$

where the index (s) designates the nature of the external drives; e.g., s = 0 designates a monopole-like and s = 1 designates a dipole-like external drives. [cf. Equation (7a).] The reflection coefficient may be elaborated to be dependent not only on the frequency variable (ω) but also on the normalized wavevector $(\mathbf{k})$; however, as already stated, this elaboration is not pursued here. Nonetheless, since there are no spatial-temporal discontinuities in the elements that compose the complex dynamic system, a spectral component in the external drive is spectrally duplicated in the component that emerges on the interface with the top fluid. This condition renders the normalized wavevector $(\mathbf{k})$ a function of the normalized frequency; namely, $\mathbf{k} = \mathbf{k}(\omega)$. Moreover, if the spectral component that one seeks on the interface with the top fluid is to be supersonic, then $|\mathbf{k}(\omega)| = k(\omega) < \omega$. These conditions are incorporated in the formalism in this report. In particular

$$k(\omega) = (\omega) \sin(\theta) \quad , (8)$$

where the angle (θ) is the directional designation of a (supersonic) component on the interface with the top fluid (fluid no. 1). Finally, the normalized surface impedance of the plate is expressed in the form

$$Z_p(k,\omega) = i\left[(1-i\eta_m)-(k^2/\omega\omega_c)^2(1+i\eta_p)\right] \quad , (9)$$

where the plate is assumed to be isotropic and (η_m) and (η_p) are, respectively, the mass-control and the stiffness-control loss factors in the plate and one is reminded, yet again, that (k), (ω_c) and (ω) are the normalized wavenumber, the normalized critical frequency and the normalized frequency, respectively. The normalizing factors are (ω_o/c_1), (ω_o) and (ω_o), respectively. Under all these assumptions and definitions, the transfer function $T_{bc}(\mathbf{k},\omega)$ is, in fact, isotropic

$$T_{bc}(\mathbf{k},\omega) \Rightarrow T_{bc}(k,\omega) \quad ; \quad k = k(\omega) \quad , (1b)$$

as can be readily verified reviewing Equations (1) - (9). A few asymptotic forms for Equation (1) are useful. These are: The coating is removed by rendering $|Z_c|$ infinite; $|Z_c| \Rightarrow \infty$. Equation

(1) then yields the transfer function $T_b(k,\omega)$ in the absence of coating to be

$$T_b(k,\omega) = Z_{f1}(k,\omega)G(k,\omega)C(k,\omega) \quad ; \quad |Z_c| \Rightarrow \infty \qquad , (10)$$

where the subscript (c) for the presence of the coating is removed and $G(k,\omega)$ is reduced to

$$G(k,\omega) \Rightarrow [Z_{f1}(k,\omega) + Z_p(k,\omega) + Z^b_{f2}(k,\omega)]^{-1} \qquad . (11)$$

[cf. Equations (2)-(9).] The baffle may be removed by rendering the reflection coefficient $R(\omega)$, at the baffle interface with the bottom fluid (fluid no. 2), equal to zero; i.e., $R(\omega) \Rightarrow 0$. This removal renders $A(k,\omega)$ and $B(k,\omega)$ equal to unity; clearly, neither is the fluid loading nor is the external drive modified in this case. The multiple reflections in the cavity that control these modifications are, of course, absent in the absence of the cavity. When $R(\omega) \Rightarrow 0$, the transfer function $T_c(k,\omega)$, in the absence of the cavity, but in the presence of the coating, reduce, from Equation (1) to

$$T_c(k,\omega) = Z(k,\omega)G(k,\omega) \quad ; \quad R(\omega) \Rightarrow 0 \qquad ,(12)$$

where the subscript (b) for the presence of the cavity is removed and $Z_{f2}^{b}(k,\omega), A(k,\omega)$ and $C(k,\omega)$ are reduced to

$$Z_{f2}^{b}(k,\omega) \Rightarrow Z_{f2}(k,\omega) \;\; ; \;\; A(k,\omega) = 1 \;\; ; \;\; C(k,\omega) \Rightarrow 1 \qquad ,(13)$$

respectively, and the normalized admittance $G(k,\omega)$ is reduced to

$$G(k,\omega) = [Z(k,\omega) + Z_p(k,\omega) + Z_{f2}(k,\omega)]^{-1} \qquad .(14)$$

[cf. Equations (2)-(9).] If, in addition, the coating is removed; i.e., $|Z_c| \Rightarrow \infty$, then the transfer function $T_c(k,\omega)$ further reduces, from Equation (12), to be

$$T(k,\omega) = Z_{f1}(k,\omega)G(k,\omega) \quad ; \quad |Z_c| \Rightarrow \infty \qquad ,(15)$$

where, in addition, the subscript (c) for the presence of the coating is removed and $G(k,\omega)$ assumes the reduced form

$$G(k,\omega) \Rightarrow [Z_{f1}(k,\omega) + Z_p(k,\omega) + Z_{f2}(k,\omega)]^{-1} \quad . (16)$$

[cf. Equations (2)-(9).] Specifying a simple coating such that (K_c) and (η_c) are mere constants, independent of the normalized frequency, Equations (1), (10), (12) and (15) are employed to compute $|T_{bc}(k,\omega)|$, $|T_b(k,\omega)|$, $|T_c(k,\omega)|$ and $|T(k,\omega)|$, respectively, as functions of the normalized frequency (ω), remembering that $k = (\omega)\sin(\theta)$. These computations are investigated next.

III. Resonances are allowed to roam

The standard computations are presented in Figure 2. These computations are carried out with the standard values: $(\eta) = (10^{-2})$, $(\eta_c) = (10^{-2})$, $(\eta_m) = (10^{-2})$, $(\eta_p) = (10^{-2})$, $(s) = 1$, $(\omega_c) = (10)$, $(k) = (0)$, $(b_1) = (0)$ and $(b) = (\pi)$, in place. Also when the standard baffle is present, the modulus of the reflection coefficient $|R(\omega)|$ is well nigh equal to unity, implying thereby that the absorption in the surface of the baffle is negligible. On the other hand, the standard removal of the baffle is accomplished by rendering the modulus of the reflection coefficient $|R(\omega)|$ negligible, implying, thereby, that the absorption in the surface of the baffle is well nigh total. Imposing these standard values to obtain Figure 2, Figure 2 exhibits characteristically the following results:

Figure 2.1 depicts $|T_{bc}(o,\omega)|$ in the solid curve and $|T_c(o,\omega)|$ in the dotted curve,

Figure 2.2 depicts $|T_b(o,\omega)|$ in the solid curve and $|T(o,\omega)|$ in the dotted curve,

Figure 2.3 depicts $\left|T_{bc}(o,\omega)\,/\,T_b(o,\omega)\right|$ in the solid curve and $\left|T_c(o,\omega)\,/\,T(o,\omega)\right|$ in the dotted curve.

The footprints of the cavity are clearly demonstrated in both, Figure 2.1 in the presence of the coating and Figure 2.2 in the absence of the coating. The influence of the coating is accentuated in Figure 2.3 where the ratio of the transfer functions in the presence of the coating to those in the absence of the coating are depicted; i.e., the curves in Figure 2.1 are divided by those in Figure 2.2 to obtain Figure 2.3. Evidently, the resonances and the anti-resonances that the cavity generate dominate the scenes in Figure 2. In the presence of the cavity, the computed results are depicted by the solid curves. Also clearly, the resonances and anti-resonances are absent in the absence of the baffle and, therefore, in the absence of the cavity. [The absence of the cavity may be achieved by rendering (b) infinite; i.e., the baffle is removed onto a plane an infinite normalized distance below the plate. The transition from a finite normalized spatial extent, in which resonances and anti-resonances are generated, to the semi-infinite normalized spatial extent in which resonances and anti-resonances are absent is thus demonstrated [21].] In the absence of the

cavity, the computed results are depicted by the dotted curves. Figures 3-5 repeat Figure 2 except that the loss factor (η) in the cavity is increased from the standard value of (10^{-2}) in Figure 2 to (10^{-1}) in Figure 3 and to (3×10^{-1}) in Figure 4 and, finally, to (5×10^{-1}) in Figure 5. Indeed, in Figures 3-5 the resonances and the anti-resonances are suppressed more and more by these successive increases in damping. In Figures 4 and 5, respectively, the resonances and the anti-resonances are further and even further suppressed than they are in Figure 3. However, the phenomenon of suppressed resonances and anti-resonances is not missing in Figure 2. The suppression in Figure 2 occurs merely at a higher frequency range than in Figure 3. To explain this phenomenon one recalls that the degree of damping is not sufficiently stated by merely specifying the loss factor [1, 2, 15]. One must also specify the normalized frequency separation $(\Delta\omega)$ between adjacent resonances. A modal overlap parameter (B) may then be defined formally as

$$B(\omega)=(\omega\eta_e/\Delta\omega)=(\omega\eta_e)\mathrm{n} \quad ; \quad \Delta\omega=[\mathrm{n}]^{-1} \quad ; \quad \mathrm{n}=\mathrm{n}(\omega) \quad ; \quad \eta_e=\eta_e(\omega) \qquad , (17a)$$

where $n(\omega)$ is the local (normalized) modal density and $\eta_e(\omega)$ is the corresponding local effective loss factor in the dynamic system. [It is recognized that $(\omega\eta_e)$ is the normalized frequency bandwidth of a local resonance or a local anti-resonance.] The degree of damping is then defined in terms of (B) in the form

$$B = \begin{cases} << 1, \text{ light damping} & ,(18a) \\ \cong 1, \text{ mid-damping} & ,(18b) \\ >> 1, \text{ high damping} & .(18c) \end{cases}$$

In the frequency locality where the local (B) is less than unity, resonances and anti-resonances dominate the scene. In the frequency locality where the local (B) is about unity, resonances and anti-resonances are just indistinguishable. Finally, in the frequency locality where the local (B) exceeds unity, resonances and anti-resonances are well nigh suppressed. In Figure 2 in the presence of the cavity the modulus of the reflection coefficient $|R(\omega)|$ is conditioned to be well nigh equal to unity, throughout the normalized frequency range of interest here; namely, $0.1 < \omega < 10^2$. Thus, the modal overlap

parameter $B(\omega)$ is dominated by the volume (bulk) loss factor (η). This $B(\omega)$ is given by

$$B(\omega) \Rightarrow B_o(\omega) = (\omega\eta)\,\mathrm{n} \quad ; \quad k = \omega\sin(\theta) = 0 \qquad .(17b)$$

[cf. Appendices.] In Figure 2 both, the loss factor (η) and the normalized modal density (n), are assumed to be independent of (ω) so that the modal overlap parameter $B_o(\omega)$ is simply proportional to (ω). This simple proportionality explains the gradual suppression of the resonances and the anti-resonances as the normalized frequency (ω) increases. In fact, the normalized frequency increases to render (B_o) in excess of unity, the suppression is complete. This phenomenon is, indeed, exhibited in Figure 2. The successive increases in (η), depicted in Figures 3-5, introduce suppressions of the resonances and the anti-resonances similar to those exhibited in Figure 2. However, compared with Figure 2, the suppressions in Figures 3-5 suffer proportional shifts to lower and lower frequencies along the normalized frequency axis as (η) increases successively. [cf. Appendix A and it is noted that since n = 1 in Figures 2-5, the modal overlap parameters are, in fact, governed by

$B_o(\omega) = (\omega\eta)$.] The suppressions are shifted successively to the lower and lower normalized frequency range. A rough estimate in Figures 2-5 would convince one that Equations (17) and (18), in the text, and Equations (A1) - (A8), in Appendix A, appear to be validated. In addition to confirming these equations, it emerges in Figures 2-5 that in those regions of the normalized frequency domain where the local modal overlap parameter (B_o) exceeds unity, the solid curve locally coalesces with the dotted curve. It is recalled that the solid curve pertains to the presence of the cavity and the dotted curve pertains to the absence of the cavity. This local coalescence of the two curves, exemplifies "The mean-value method of predicting the dynamic response of complex vibrations" proposed by Skudrzyk [20].

It has been established that there exists a reasonable correspondence between the absorption in the surface of the baffle and the volume (bulk) absorption represented by the loss factor (η). In this vein, it may be useful to cast the modulus of the reflection coefficient $|R(\omega)|$ in the form

$$|R(\omega)| \Rightarrow |R| = \exp[-(r_b)] \quad , (19a)$$

where (r_b) is positive, is real and is assumed to be independent of (ω). Thus, in Figures 2-5 the value of (r_b) is conditioned to be equal to (10^{-3}), rendering $|R|$ substantially equal to unity. The value of $r_b = (10^{-3})$ is designated standard. The standard value of (r_b) is changed in a manner reminiscent of the changes in (η) depicted in Figures 3-5. The changes in (r_b) are from the standard value of (10^{-3}) to $(2\pi \text{ x } 10^{-1})$ to (2) and, finally, to (π). The influence of these changes is depicted in Figures 6-8, respectively, with Figure 2 serving as the standard base. In Figures 6-8 the volume loss factor (η) is maintained at the standard value of (10^{-2}). Therefore, only at the higher normalized frequency range, where $\omega > 50$, does the value of (B_o) approach unity. As explained in Appendix A the contribution of $B_b(\omega)$ to the modal overlap parameter $B(\omega)$ by the absorption at the surface of the baffle is given by

$$B(\omega) = B_b(\omega) + B_o(\omega) \quad ; \quad B_b(\omega) = (r_b/2\pi) \quad ;$$
$$k = \omega \sin(\theta) = 0 \qquad .(17c)$$

The increases in (r_b) that are depicted in Figures 6-8 are compared with the corresponding increases in (η) in Figures 3-5, respectively. Figures 6-8 and Figures 3-5 show similar departures from Figure 2. Moreover, the features in Figures 6-8 can be similarly interpreted in the light of Figures 3-5 vis-à-vis Figure 2. Indeed, the absorption in the surface of the baffle are quite similar to the absorption in the body of the fluid (fluid no. 2) in the cavity, not a surprising similarity to a noise control engineer. The difference lies in that the influence of the loss factor in the function $[\exp\{a(k,\omega)\}]$ is made frequency dependent, whereas the reflection coefficient, as assumed here, is not so influenced. In particular, from Equation (7), and with the assistance of Appendix A, one finds

$$\left|\exp\{a(k,\omega)\}\right| = \exp\left[-2\,(\omega\eta)(c_1/c_2)(b)\,k_{32}(k,\omega)\right] \quad ;$$

$$k = \omega\sin(\theta) \quad ; \quad 0 \le \theta < (\pi/2) \qquad , (19b)$$

where (η) is assumed to be largely frequency independent and (b) is the normalized separation between the plate and the baffle; i.e., (b) is the normalized width of the cavity. Comparisons between Figures 6-8 and Figures 3-5, respectively, reveal that differences in details exist. Although the differences may be

adequately interpreted by the material presented in Appendix A, dealing with these differences, in addition to the above discussion, is, however, beyond the scope of this report.

IV. Deroaming the resonances (and anti-resonances) by converting summations to integrations

One learnt that the damping, including that contributed by the absorption in the surface of the baffle, tends to converge the solid curves onto the dotted curves in Figures 2-8. The convergence is particularly complete in those ranges of the frequency for which the local modal overlap parameters exceed unity. It is proposed that the action of converting summations over modes to integrations is equivalent to increasing the value of the modal overlap parameters in those locations in the frequency domain in which the inherent value of the modal overlap parameters lie below unity. By contrast, in those regions in the frequency domain in which the value of the local modal overlap parameters exceed unity, converting summations to integrations is obviously and properly authorized. In these regions the integrations are commensurate with the summation over a well nigh continuous distribution of modes [13, 14]. The continuity, it is emphasized, is conditioned by the value of the local modal overlap parameters that exceed unity; neither the value of the local (normalized) modal densities alone nor the value of the local loss factors alone will suffice to ensure this continuity [15]. How is that to be interpreted? From Figures 2-8 as just stated, the absorption in the cavity tends

to bring the solid curves to converge onto the dotted curves. This convergence is completed when the absorption is high enough to be commensurate with the removal of the cavity. This removal may be in the form of increasing (b) to infinity which amounts to gradually rendering the bottom fluid (fluid no. 2) semi-infinite. Recall that the top fluid (fluid no. 1) is a initio semi-infinite. When the increase is final the solid curves are then coincident with the dotted curves [21]. It is also observed in Figures 2-8 that the excursions in the solid curves, manifesting the resonances and the anti-resonances, diminish as the value of the local modal overlap parameter $B(\omega)$ increases toward unity, notwithstanding that the dotted curves remain unchanged by these increases in $B(\omega)$. Indeed, it is observed in these figures that the dotted curves serve as the geometrical mean to the positive excursions of the resonances with the negative excursions of the adjacent anti-resonances. [It is to be recalled that resonances and anti-resonances form adjacent pairs.] This geometrical mean then remains unchanged by (reasonable) changes in the value of the local modal overlap parameter $B(\omega)$. Thus, as far as this geometrical mean is concerned, resonances and anti-resonances may be artificially added and modified to close the gaps between adjacent peaks and

nadirs even in those frequency regions where $B(\omega)$ is less than unity. These insertions and modifications, which result in higher modal densities and/or in higher loss factors, may effectively render $B(\omega)$ in excess of unity in any desired region in the frequency domain. This rendering a priori causes the solid curves to be coincident with the dotted curves. Thereby, indicating that in this region the resonances and the anti-resonances are indistinguishable and the transition along the normalized frequency axis is smooth. It is this contrived smoothness that allows one to convert the thorny summations into integrations. After all, the allowed artificial insertions and modifications of resonances and anti-resonances render the modal distribution well nigh continuous. Conversely, when summations are converted to integrations this artificial insertion and modification of resonances and anti-resonances is implied a priori. Can this contention be illustrated by analysis and by computations? To illustrate, one needs to revisit Equation (7). The summations in these equations are associated with the resonances and the anti-resonances that are generated by the factors that represent summations. These factors and their representation by summations are

$$[1 + R(\omega)\ \exp\{a(k,\omega)\}]^{-1} = \sum_{m=0}^{\infty} [-R(\omega)\ \exp\{a(k,\omega)\}]^m \qquad , (20a)$$

$$[1 - R(\omega)\ \exp\{a(k,\omega)\}]^{-1} = \sum_{m=0}^{\infty} [R(\omega)\ \exp\{a(k,\omega)\}]^m \qquad , (20b)$$

$$[1 + (-1)^s R(\omega)\ \exp\{as(k,\omega)\}]^{-1}$$

$$= \sum_{m=0}^{\infty} [(-1)^{s+1} R(\omega)\ \exp\{as(k,\omega)\}]^m \qquad , (20c)$$

where one is reminded that (s) is an index designating the pole nature of the external drives; e.g., s = 0 designates monopole-like and s = 1 designates dipole-like external drives. The conversion of these summations to integrations yields

$$[1 + R(\omega)\ \exp\{a(k,\omega)\}] \Rightarrow 1 \qquad , (21a)$$

$$[1 - R(\omega)\ \exp\{a(k,\omega)\}] \Rightarrow 1 \qquad , (21b)$$

$$[1 + (-1)^s R(\omega) \exp\{as(k,\omega)\}] \Rightarrow 1 \qquad , (21c)$$

respectively, where use is made of the identity

$$\ln[X(k,\omega)]\int_{O}^{\infty}[X(k,\omega)]^{Y}\,dy = 1 \qquad .(22)$$

Substituting Equation (21) in Equation (7) yields $A(k,\omega)$ and $C(k,\omega)$ to be equal to unity. This substitution then renders

$$T_{bc}(k,\omega) \Rightarrow T_c(k,\omega) \quad ; \quad T_b(k,\omega) \Rightarrow T(k,\omega) \qquad ,(23)$$

respectively. Equation (23) may be verified employing Equations (1) and (12) and Equations (10) and (15), respectively. As contended, the conversion of the summations to the corresponding integrations, indeed, suppresses the resonances and anti-resonances in the transfer functions of concern. Again, examining Equation (21) reveals that this suppression is commensurate with assigning a total absorption at the baffle, which renders $|R(\omega)| \Rightarrow 0$. This condition, in turn, is commensurate with the removal of the cavity. The conditions that are obeyed in Figure 2 are augmented by Equation (21) and the moduli of the transfer functions $|T_{bc}(k,\omega)|$, $|T_b(k,\omega)|$, $|T_c(k,\omega)|$ and $|T(k,\omega)|$, are computed. The results of these computations are depicted in Figure 9. The solid curves in Figure 9 are those in Figure 2 except that the summations are converted to the corresponding integrations as prescribed in

Equations (20) and (21). A comparison of Figure 9 with Figure 2 would rest the contention made in this section, if not in the paper as a whole. Nonetheless, for the record, it may be useful to restate the contention in bolder terms. Equations (1), (7), (20) and (21), in unison, declare that the transfer functions, when summations are converted to corresponding integrations, become independent of the effective loss factor (η_e). This loss factor describes the sum of both, volume and surface, absorptions in the cavity; $\eta_e = (\eta_b + \eta)$. This independence, it was argued, allowed one to assume that (η_e) may be set as small as one wishes, without changing the transfer functions [15-19]. Setting (η_e) small, without invoking a proper criterion to computing Figure 9, may be misleading, as Figure 10 attests. Figure 10 repeats Figure 2 except that, whereas (r_b) remains equal to (10^{-3}), (η) is changed from the standard value (10^{-2}) in Figure 2 to (10^{-4}) in Figure 10. The ratio of the effective loss factor $(\eta_e)_{10}$ in Figure 10 to the effective loss factor $(\eta_e)_2$ in Figure 2 is then

$$[(\eta_e)_{10}/(\eta_e)_2] = [(5/\pi) + \omega][(5/\pi) + 10^2\omega]^{-1} << 1 \quad ;$$

$$0{\cdot}1 < \omega < 10^2 \qquad .(17d)$$

Under the criterion for converting the summations to integrations, Figure 9 is common to Figures 10 and 2 [7]. Yet, Figure 9 does not only hide the presence of resonances and anti-resonances in Figure 2, but it hides the differences between Figure 2 and Figure 10. These differences are accounted for by Equation (17d). What would Figure 9 hide were one tempted to render the effective loss factor (η_e) vanishingly small [1, 2]?

Finally, both, the resonances and anti-resonances, are prominently present in the foregoing considerations. In most practical situations, even when the resonances are clearly distinguishable, the anti-resonances are usually obscured by noise. Thus, the peaks in the resonances may be simply visible and identified, but the nadirs in the anti-resonances are hidden within the noise. The geometrical averaging, is therefore, not readily implemented. The averaging that is usually implemented under these circumstances tends to rise above the geometrical average. As argued, a noise control measure; e.g., increase in damping, will tend to bring the response, as expressed, for example, by the transfer function here considered, toward the geometrical mean a'la Skudrzyk [7]. In practice, the increase in damping also will cause an increase in the levels of the nadirs of the anti-resonances. This *demerit*, however, is

obscured by the noise. (What the eye does not see, the heart does not grieve!) The merit of the damping, in the initial stages of increasing it may, thereby, be exaggerated. Nonetheless, once the geometrical mean-level has been reached, further increases in damping, that will increase the modal overlap parameter beyond unity, would be of no practical benefit. The resonances and the anti-resonances can hardly reverse their roles and a beneficial saturation will prevail.

Appendix A

In order to carry out a number of computations it becomes necessary to state more explicitly the parameters that define the dynamic system. Of particular significance are the analytical forms for the normalized modal densities and the loss factors. Through these parameters, the analytical expressions for the modal overlap parameters may then be derived. In this vein, the normalized modal density $n(\omega)$ of the resonances (and of the anti-resonances) in the dynamic system here considered may be simply ascertained. [The modal density is the inverse of the frequency separation $(\Delta\omega)$ between adjacent resonances. The *normalized* modal density pertains to the *normalized* frequency separation.] For this purpose the reflection coefficient (R) is cast in the form

$$R(\omega) = \exp[-r_b(\omega) - ir_I(\omega)] \quad , (A1)$$

with (r_b) and (r_I) real parameters. Recalling Equation (7) the local (normalized) modal density $n(\omega)$ assumes, by definition, the expression

$$[2\pi \mathrm{n}(\omega) - \{\partial r_I(\omega)/\partial\omega\}] = A_b \quad ; \quad k = k(\omega) < (\omega/c_1) \quad ;$$

$$A_b = 2\,(c_1/c_2)(b)[k_{32}(k,\omega)] \qquad , \text{(A2)}$$

where it is assumed that the normalized depth (b) of the cavity is independent of the normalized frequency (ω) and the normalized wavenumber (k) is restricted to the supersonic range; in this case $k_{32}(k,\omega) \Rightarrow k_{32}[\omega \sin\theta, \omega]$. Again the angle (θ) is the direction, off the normal to the plane of the plate, of radiation into the top fluid (fluid no. 1) by the emerging supersonic component on the interface with that top fluid.

Similarly, an *equivalent volume* (or bulk) loss factor may be defined to account for the absorption in the surface of the baffle. This local loss factor is designated (η_b) and the expression for it is

$$(\omega\eta_b) = [r_b(\omega)/A_b] \quad ; \quad k = k(\omega) < \omega \qquad . \text{(A3)}$$

In this connection, (η) is the volume (or bulk) loss factor in the cavity. The local modal overlap parameter $B(\omega)$, in the

cavity here considered, may then be determined in the two-components form

$$B = B_b + B_o \quad ; \quad B_b = (\omega \eta_b) \mathrm{n}(\omega) \quad ; \quad B_o = (\omega \eta) \mathrm{n}(\omega) \qquad . (A4)$$

[cf. Equation (17).] Substituting Equations (A2) (A3) and (A4) in the factor $[R(\omega) \exp \{\mathrm{a}(k, \omega)\}]$ in Equation (7), one may show that the absolute value of this factor may be cast in the form

$$\left| R(\omega) \exp \{\mathrm{a}(k, \omega)\} \right| = \exp[-\{\omega \eta_e(\omega)\} A_b] \quad ;$$

$$\eta_e(\omega) = \eta_b(\omega) + \eta(\omega) \qquad . (A5)$$

where $\eta_e(\omega)$ is the effective loss factor in the cavity. [cf. Equation (17a).] Merely for the sake of simplicity and convenience (r_I), (r_b) and (η) are assumed to be largely independent of (ω). It is further decreed that the computations are to be carried out for components for which

$$k = \omega \sin(\theta) \quad ; \quad k_{32}(k, \omega) = k_{32}[\omega \sin(\theta), \omega] \qquad , (A6a)$$

and if $c_1 = c_2$ then

$$k_{32}(k,\omega) = k_{32} = \cos(\theta) \quad , \text{(A6b)}$$

and, therefore, (k_{32}) is independent of the normalized frequency (ω) and the angle (θ) is the directional designation of a (supersonic) component on the interface with the top fluid (fluid no. 1). Imposing Equations (A6b) on Equation (A5) reduces this equation to read

$$\left|R(k,\omega)\exp\{a(k,\omega)\}\right| \Rightarrow \exp\left[-\{r_b + (\omega\eta)A_b\}\right] \quad ;$$

$$A_b \Rightarrow 2\left[(b)\cos(\theta)\right] \quad , \text{(A7)}$$

and then one finds that

$$(\omega\eta_b) = (r_b/2)[b\cos(\theta)]^{-1} \quad ; \quad n = (\pi)^{-1}[b\cos(\theta)] \quad ;$$

$$B_b = (r_b/2\pi) \quad ; \quad B_o = (\omega\eta)(\pi)^{-1}[b\cos(\theta)] \quad . \text{(A8)}$$

Appendix B

In this appendix a number of variations on the theme are illustrated. The purpose is to show the versatility of the computational breadth of the analysis. However, this analysis is used here exclusively toward the arguments that lie within the scope chosen for this report. The analysis and the model employed could, in the future, serve a wider and a more extended scope. In this vein, in Figure B1, Figure 2 is repeated except that the external drives are changed from the standard dipole-like with $s = 1$, to a monopole-like, with $s = 0$. [cf. Equation (7b).] The influence of this change can be observed in comparing Figure 2 with Figure B1. There is a difference not only in the dispositions of the resonances and anti-resonances but also in their excursions at the higher frequency ranges. Indeed, they converge more slowly on to the geometrical mean with increase in frequency than when $s = 0$. However, the difference is insignificant to the arguments conducted in this report. To emphasize this point Figure B2 is shown. In this figure, Figure 3 is repeated with $s = 0$. The relationship between Figures B1 and B2 are similar to those between Figures 2 and 3. On the same theme Figure B3 is offered. The external drives which are placed in Figure 2 on the standard plane at (b_1)

equal to zero, are now placed at $(b_1) = 0.2b$. Again, there is a difference between Figure 2 and Figure B3 that is similar, in certain aspects, to the difference between Figure 2 and Figure B1. This difference is also insignificant to the arguments conducted in this report. This point is further emphasized in Figure B4. In this figure, Figure 3 is repeated except that the conditions that $b_1 = 0$ is replaced by $b_1 = 0{\cdot}2b$. Again, the relationship between Figures 2 and 3 are similar to those between Figures B3 and B4.

Another variation on the theme deals with a change in the normalized wavenumber (k) from the standard value of zero in Figure 2 to the value of $(\omega\sqrt{3}/2)$ in Figure B5. The latter value of (k) defines the components on the interface with the top fluid (fluid no. 1) that are destined to radiate into an angle (θ) of (60°) to the normal to the plane of the plate. The normalized critical frequency (ω_c), which now plays a role, is set at the standard value of ten (10) in both figures. [cf. The expression for the normalized surface impedance of the plate stated in Equation (9).] The influence of the plate switching from a mass control to a stiffness control surface impedance, within the

range of (ω) depicted in the figures, is clearly visible in Figure B5. In Figure 2 that switch never occurs. Once again, this feature in the transfer function is of little significance to the arguments pursued in this report.

A more potent case is presented in Figure B6. In this figure the normalized depth (b) of the cavity is rendered (artificially) dependent on the normalized frequency (ω); instead of the standard value of $(b) = \pi$ in Figure 2, it is changed to the value of $(2\pi / \sqrt{\omega})$ in Figure B6 and, in particular, the speeds in the fluids remain equal; $c_1 = c_2$. Clearly, Figure 2 differs from Figure B6 in that the modal density of the resonances (and of the anti-resonances) is changed from that of

$$n(\omega) = (k_{32}) \equiv [\cos(\theta)] \quad ; \quad (b) = \pi \qquad , \text{(B1a)}$$

in Figure 2 to that of

$$n(\omega) = [\cos(\theta)](\omega)^{-(1/2)} \quad ; \quad (b) = 2\pi(\omega)^{-(1/2)} \qquad , \text{(B1b)}$$

in Figure B6. Similarly, in Figure 2 the modal overlap parameters (B_b) and (B_o) are

$$B_b = (r_b/2\pi) \quad ; \quad B_o = (\omega\eta)[\cos(\theta)] \qquad , (B2)$$

respectively. [cf. Equation (A8).] In Figure B6 these parameters change to read

$$B_b = [(r_b/2\pi)(1/2)] \quad ; \quad B_o = [(\omega)^{1/2}\eta][\cos(\theta)] \qquad , (B3)$$

respectively. Since (r_b) is small; $r_b = 10^{-3}$, in both, Figures 2 and B6, (B_b) plays a minor role in these figures. Then only the change in (B_o) is significant; in Figure 2 (B_o) is proportional to the normalized frequency (ω) and in Figure B6 (B_o) is proportional to the square root of the normalized frequency $(\omega)^{1/2}$. Thus, $B_o(\omega)$ is lower in the higher frequency range in Figure B6 than in Figure 2. This difference is significant to the arguments conducted in this report. Nonetheless, Figure B6 is relegated to the appendix because of its physical artificiality. Of course, the bottom fluid could be made to possess a sound speed that is dispersive; e.g.,

$c_2 = \alpha\sqrt{\omega}$ with α a constant, but, then, too many modifications to the formalism would be required. And that too lies outside the scope of this report.

Last, but not least, can the replacement of summations by integrations handle a change in the external sources? In Figure 9, s = 1. A change in (s) from one (1) to zero (0) has been made and Figure 9 emerged in this computation. It would be superfluous to show the result of this computation under a separate cover. And just to be clever, Figure 9 is repeated in Figure B7 except that the conditions on (k) are made to fit that used in Figure B5; i.e., (k) is changed from zero to $(\omega\sqrt{3}/2)$. The change in the surface impedance of the plate is clearly visible in Figure B7 as it is in Figure B5.

In passing, although obvious, it may be prudent to note that the influence of the coating remains intact to changes in (s) and in (b_1). This is made clear by comparing the solid curve in Figure 2.3 with the solid curves in Figures B1.3 and B3.3 and the solid curve in Figure 3.3 with the solid curves in Figures B2.3 and B4.3, respectively.

References

1. R. H. Lyon (1975). Statistical Energy Analysis of Dynamic Systems: Theory and Applications, (MIT, Cambridge).

2. R. H. Lyon and R. G. Dejung (1995). Theory and Application of Statistical Energy Analysis, (Butterworth-Heinemann, Boston).

3. R. S. Lanley and V. Cotoni (2004). "Response variance prediction in the statistical energy analysis of built-up systems," J. Acoust. Soc. Am. **115**, 706-718.

4. C. Soize (2001). "Variability matrix theory and non-parametric model of random uncertainties in vibration analysis," J. Sound Vib. **263**, 893-916.

5. R. H. Lyon (2001). "Variability in SEA," on the CD-ROM: *Proceedings of India-USA Symposium on Emerging Trends in Vibration and Noise Engineering. The Ohio State University, Columbus, OH. December 10-12, 2001,* edited by A. Selamet, R. Singh, and B. C. Nakra.

6. R. L. Weaver (1989). "Spectral statistics in elastodynamics," J. Acoust. Soc. Am. **85**, 1005-1013.

7. M. R. Schroeder (1962). "Frequency-correlation functions of frequency responses in rooms," J. Acoust. Soc. Am. **34**, 1819-1823.

8. G. Maidanik and K. J. Becker (2003). "Dependence of the induced damping on the coupling forms and coupling strengths: Linear Analysis," J. Sound Vib. **266**, 15-32. "Dependence of the induced damping on the coupling forms and coupling strengths: Energy Analysis," J. Sound Vib. **266**, 33-48.

9. K. L. Chandiramani (1978). "Some simple modes describing the transition from weak to strong coupling in statistical energy analysis," J. Acoust. Soc. Am. **63**, 1081-1083.

10. P. W. Smith, Jr. (1979). "Statistical modes of coupled dynamical systems and the transition from weak to strong coupling," J. Acoust. Soc. Am. **65**, 695-698.

11. R. H. Lyon (1969). "Statistical analysis of power injection and response in structures and rooms," J. Acoust. Soc. Am. **45**, 545-565.

12. G. Maidanik and J. Dickey (1997). "On the external input power into coupled structures," *Proceedings of the Symposium of Statistical Energy Analysis, IUTAM, Southampton, England.*

13. Le Chatelier's Principle (2001). The Columbia Encyclopedia, Sixth Edition, (Columbia University Press, New York) (www.bartleby.com/65/,9/12/2003) and J. B. Breckenridge and R. M. Rosenberg (1970). The Principles of Physics and Chemistry, (McGraw-Hill, New York).

14. A. Carcaterra and A. Akay (2004). "Transient energy exchange between a primary structure and a set of oscillators: return time and apparent damping," J. Acoust. Soc. Am. **115**, 683-696.

15. G. Maidanik (2000). "Induced damping by a nearly continuous distribution of nearly undamped oscillators: Linear Analysis," J. Sound Vib. **240**, 717-731.

16. M. Strasberg and D. Feit (1996). "Vibration of large structures by attached small resonant structures," J. Acoust. Soc. Am. **99**, 335-344.

17. A. Pierce, V. W. Sparrow and D. A. Russell (1995). "Fundamental structural-acoustic idealizations for structures with fuzzy internals," J. Acous. Vib. **117**, 339-348.

18. R. J. Nagem, I. Veljkovic and G. Sandri (1977). "Vibration damping by a continuous distribution of undamped oscillators," J. Sound Vib. **207**, 429-434.

19. Yu. A. Kobelev (1987). "Absorption of sound waves in a thin layer," Sov. Phy. Acous. **33**, 295-296.

20. E. Skudrzyk (1980). "The mean-value method of predicting the dynamic response of complex vibrations," J. Acoust. Soc. Am. **67**, 1105-1135.

21. M. Strasberg (1996). "Continuous structures as '*fuzzy*' substructures," J. Acoust. Soc. Am. **100**, 3456-3459.

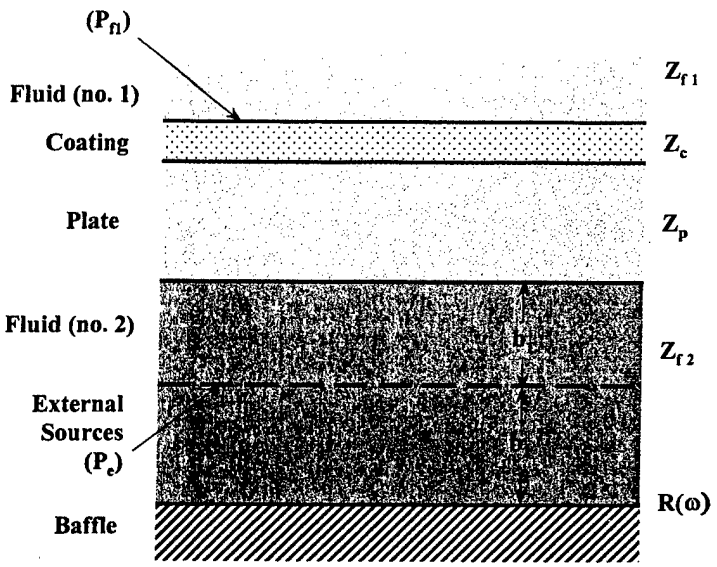

a. Elements of the Model

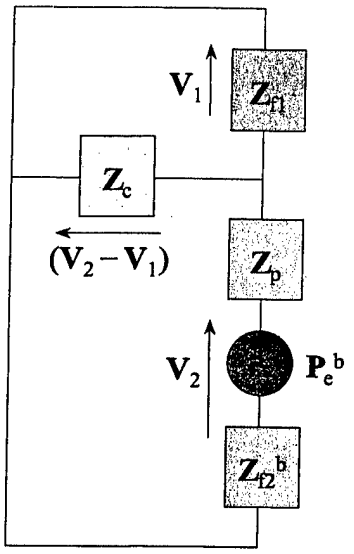

c. Equivalent Circuit Diagram

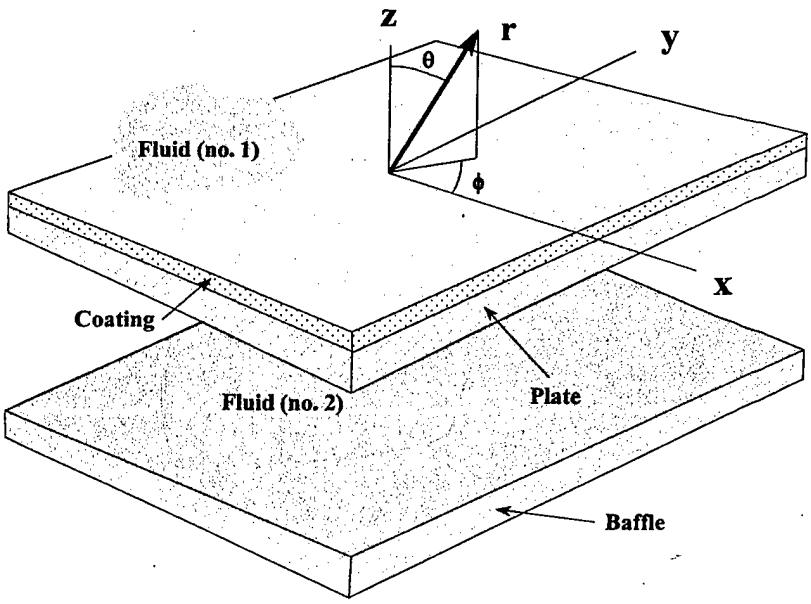

b. Physical Construction of the Model

$$\boldsymbol{Z}^{b}\boldsymbol{V} = \boldsymbol{P}_{e}^{b}$$

$$\boldsymbol{V} = \left\{V_1, V_2\right\}$$

$$\boldsymbol{P}_{e}^{b} = \left\{0, P_{e}^{b}\right\}$$

$$P_{e}^{b} = \left(Be\,P_{e}\right)$$

$$\boldsymbol{Z}^{b} = \begin{pmatrix} (Z_{f1} + Z_c) & -Z_c \\ -Z_c & (Z_c + Z_p + Z_{f2}^{b}) \end{pmatrix}$$

$$Z_{f2}^{b} = \left(Z_{f2}\,Ae\right)$$

$$P_{f1} = \left(Z_{f1}\,V_1\right)$$

d. A Brief Synopsis of the Analysis

Fig. 1

Figure 2.1. The transfer function, as a function of the normalized frequency (ω), for standard coated plate under the standard conditions: $|R(\omega)| = \exp(-10^{-3})$, $\eta = 10^{-2}$, $\eta_c = 10^{-2}$, $s = 1$, $(\omega_c/\omega_o) = 10$, $(k_o b) = \pi$, $(k_o b_1) = 0$, $(k/k_o) = 0$, fluid loading factor $\gamma = (\rho_1 c_1/m\omega_c) = 0.13$ and the fluids on both sides, fluid no. 1 and fluid no. 2, possess equal properties; i.e., $\rho_1 = \rho_2$ and $c_1 = c_2$. Note that $k_o = (\omega_o/c_1)$.

$\frac{|Tbc(k(\omega),\omega)|}{|Tc(k(\omega),\omega)|}$ .....

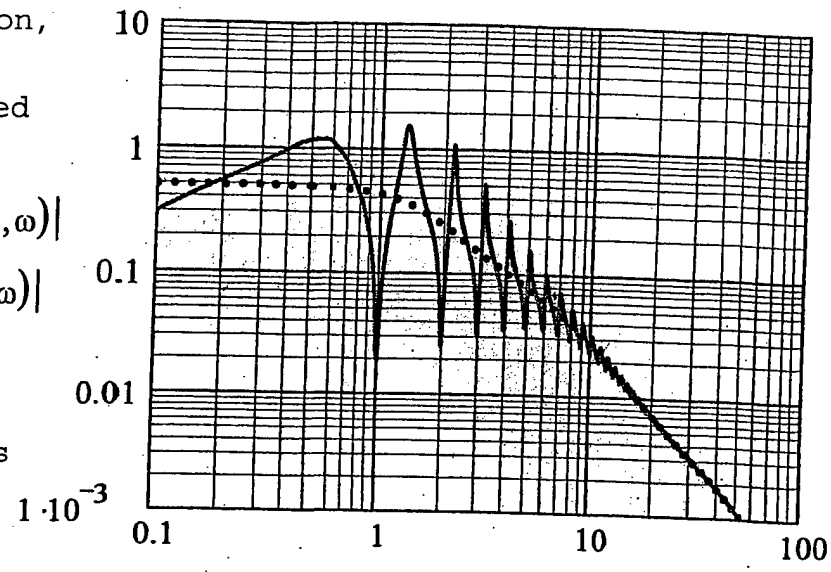

Figure 2.2. As in Figure 2.1 except that the plate is uncoated.

$\frac{|Tb(k(\omega),\omega)|}{|T(k(\omega),\omega)|}$ .....

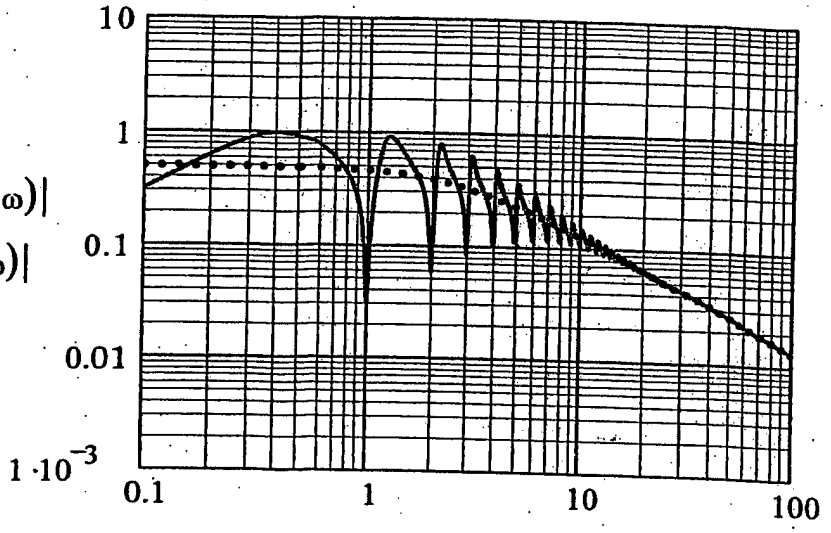

Figure 2.3. The ratio of the transfer functions, as a function of the normalized frequency (ω). The ratio is between the coated and uncoated plates; i.e., Figure 2.1 divided by Figure 2.2.

$\frac{|Tbc\_Tb(k(\omega),\omega)|}{|Tc\_T(k(\omega),\omega)|}$ .....

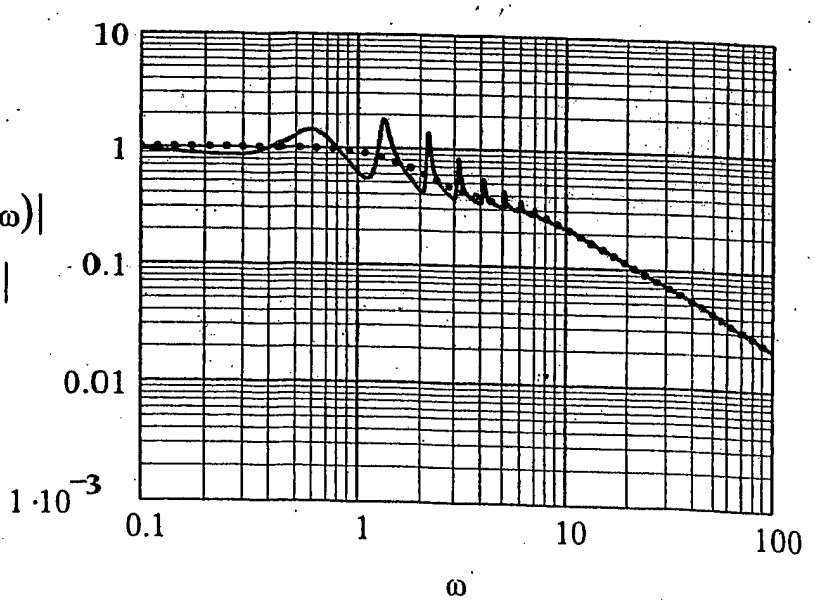

Figure 3.1. The same as Figure 2.1 except that (η) is changed from the standard value of (10^{-2}) to (10^{-1}).

$$\frac{|Tbc(k(\omega),\omega)|}{|Tc(k(\omega),\omega)|}$$

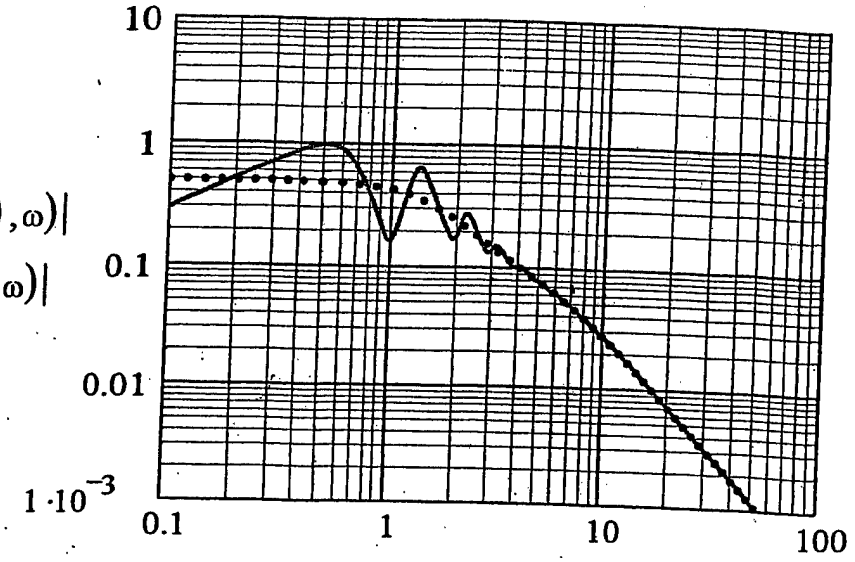

Figure 3.2. The same as Figure 2.2 except that (η) is changed from the standard value of (10^{-2}) to (10^{-1}).

$$\frac{|Tb(k(\omega),\omega)|}{|T(k(\omega),\omega)|}$$

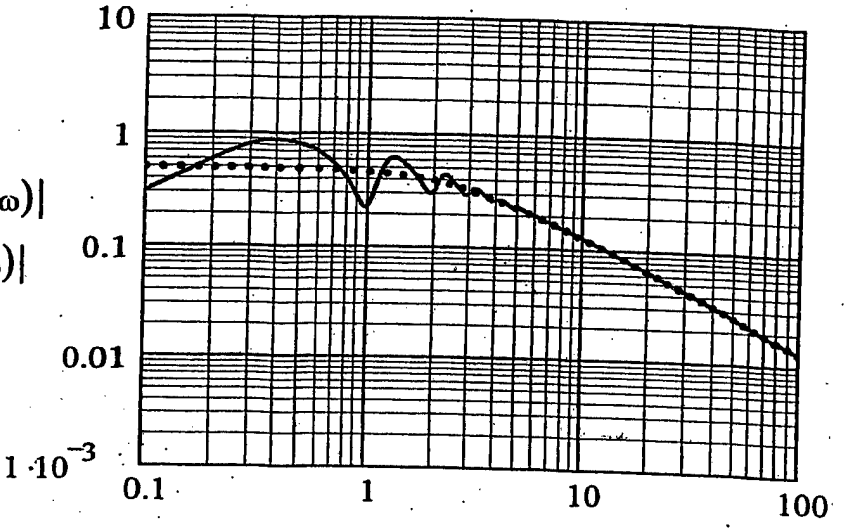

Figure 3.3. The same as Figure 2.3 except that (η) is changed from the standard value of (10^{-2}) to (10^{-1}).

$$\frac{|Tbc\_Tb(k(\omega),\omega)|}{|Tc\_T(k(\omega),\omega)|}$$

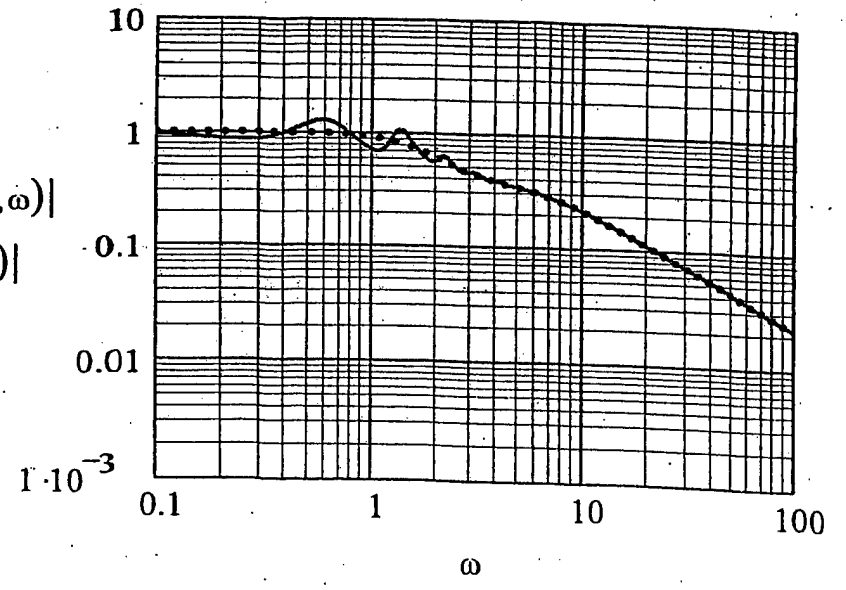

Figure 4.1. The same as Figure 2.1 except that (η) is changed from the standard value of (10^{-2}) to $(3x10^{-1})$.

$\frac{|Tbc(k(\omega),\omega)|}{|Tc(k(\omega),\omega)|}$

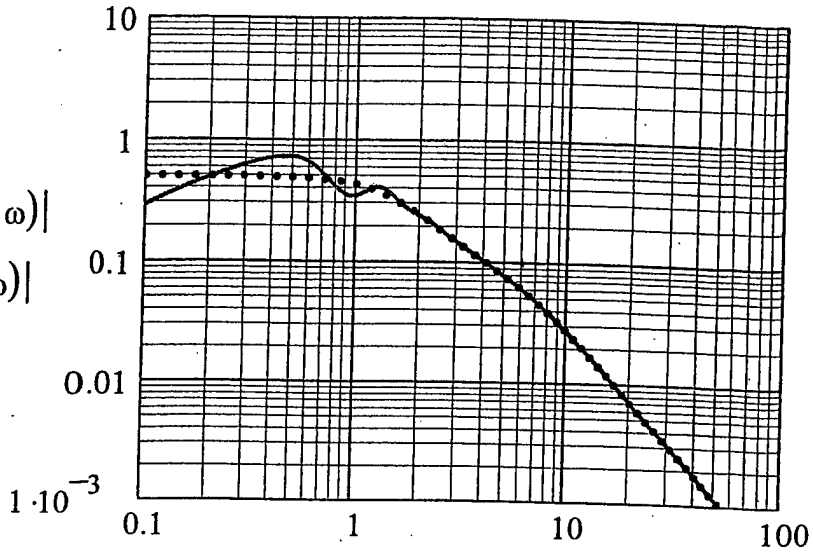

Figure 4.2. The same as Figure 2.2 except that (η) is changed from the standard value of (10^{-2}) to $(3x10^{-1})$.

$\frac{|Tb(k(\omega),\omega)|}{|T(k(\omega),\omega)|}$

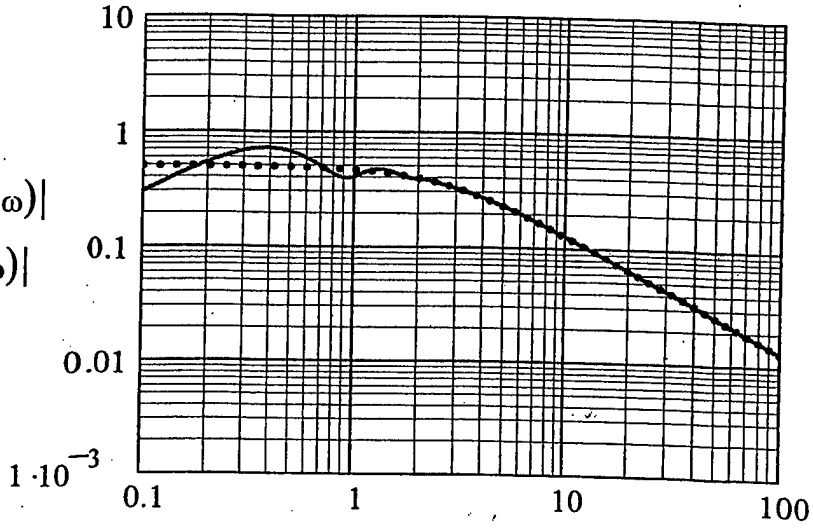

Figure 4.3. The same as Figure 2.3 except that (η) is changed from the standard value of (10^{-2}) to $(3x10^{-1})$.

$\frac{|Tbc\_Tb(k(\omega),\omega)|}{|Tc\_T(k(\omega),\omega)|}$

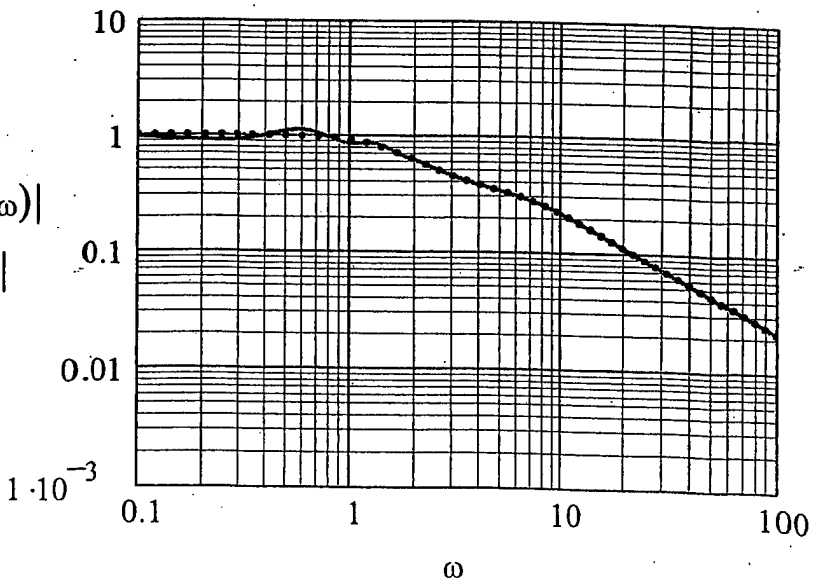

Figure 5.1. The same as Figure 2.1 except that (η) is changed from the standard value of (10^{-2}) to $(5x10^{-1})$.

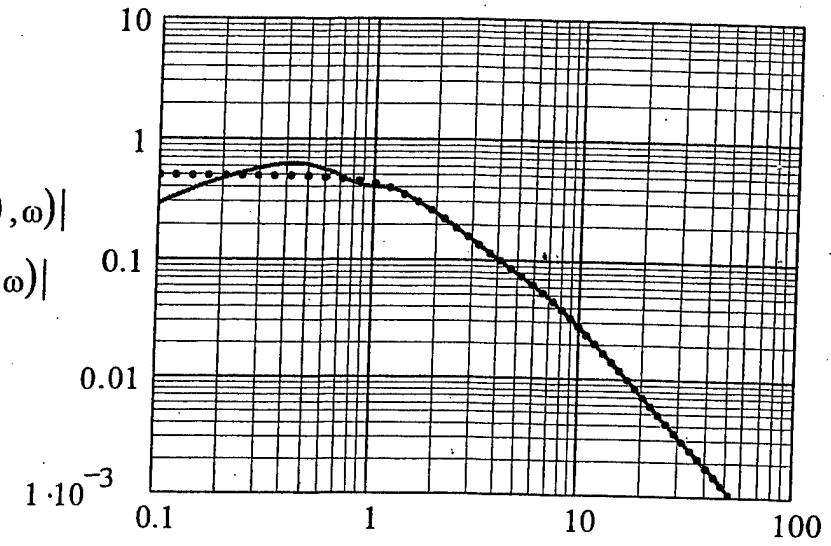

Figure 5.2. The same as Figure 2.2 except that (η) is changed from the standard value of (10^{-2}) to $(5x10^{-1})$.

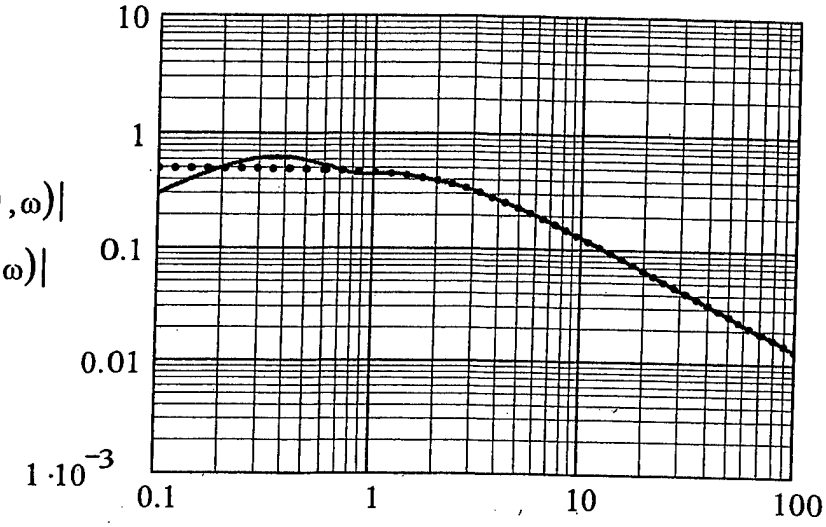

Figure 5.3. The same as Figure 2.3 except that (η) is changed from the standard value of (10^{-2}) to $(5x10^{-1})$.

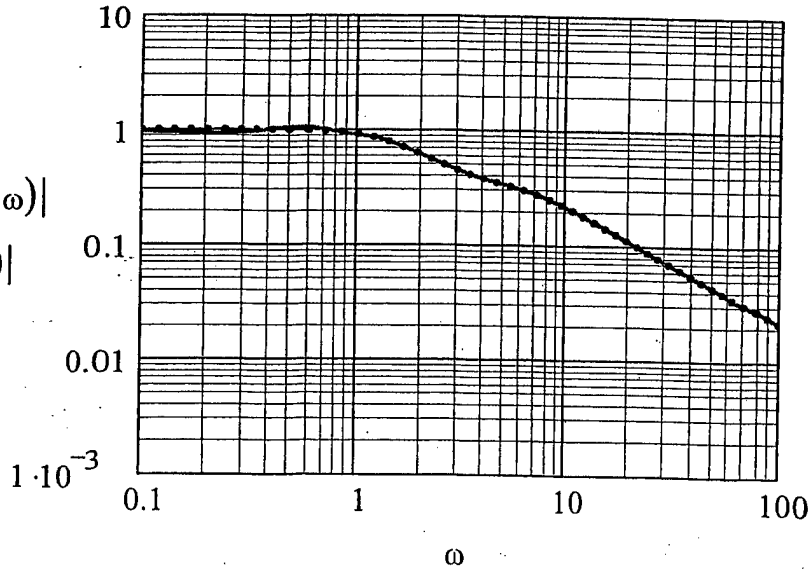

Figure 6.1. The same as Figure 2.1 except that $|R(\omega)|$ is changed from the standard value of [exp(-10^{-3})] to [exp(-2πx10^{-1})].

$\frac{|Tbc(k(\omega),\omega)|}{|Tc(k(\omega),\omega)|}$ .....

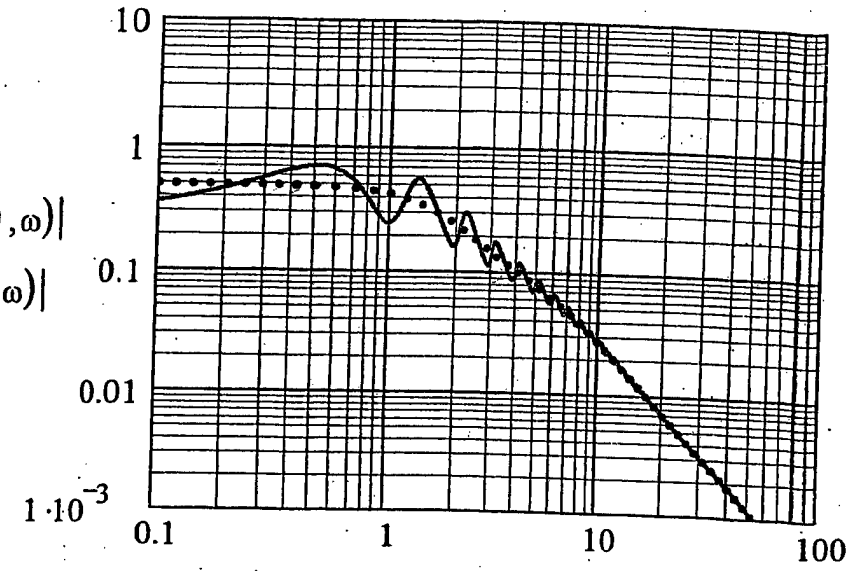

Figure 6.2. The same as Figure 2.2 except that $|R(\omega)|$ is changed from the standard value of [exp(-10^{-3})] to [exp(-2πx10^{-1})].

$\frac{|Tb(k(\omega),\omega)|}{|T(k(\omega),\omega)|}$ .....

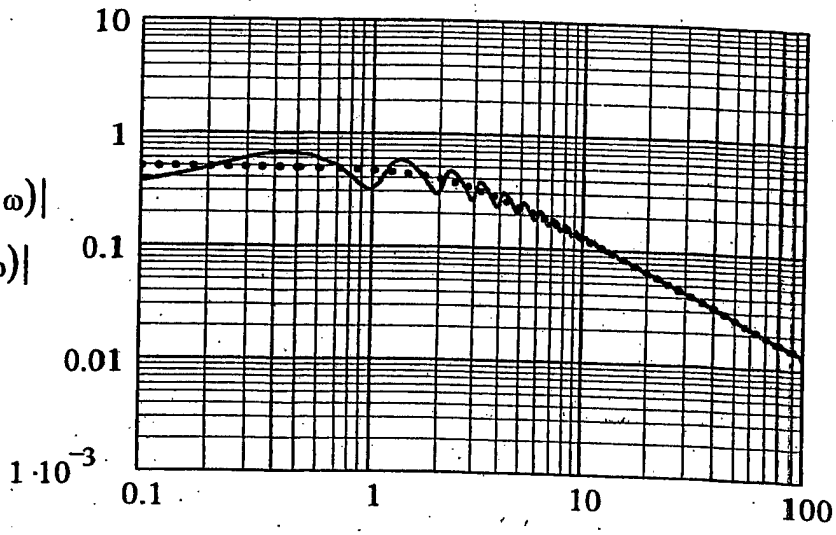

Figure 6.3. The same as Figure 2.3 except that $|R(\omega)|$ is changed from the standard value of [exp(-10^{-3})] to [exp(-2πx10^{-1})].

$\frac{|Tbc\_Tb(k(\omega),\omega)|}{|Tc\_T(k(\omega),\omega)|}$ .....

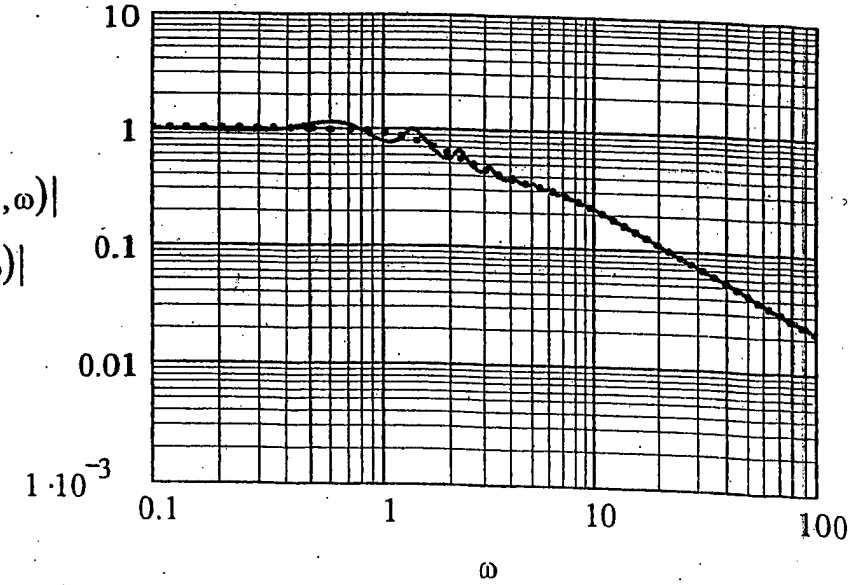

Figure 7.1. The same as Figure 2.1 except that $|R(\omega)|$ is changed from the standard value of [exp(-10^{-3})] to [exp(-2)].

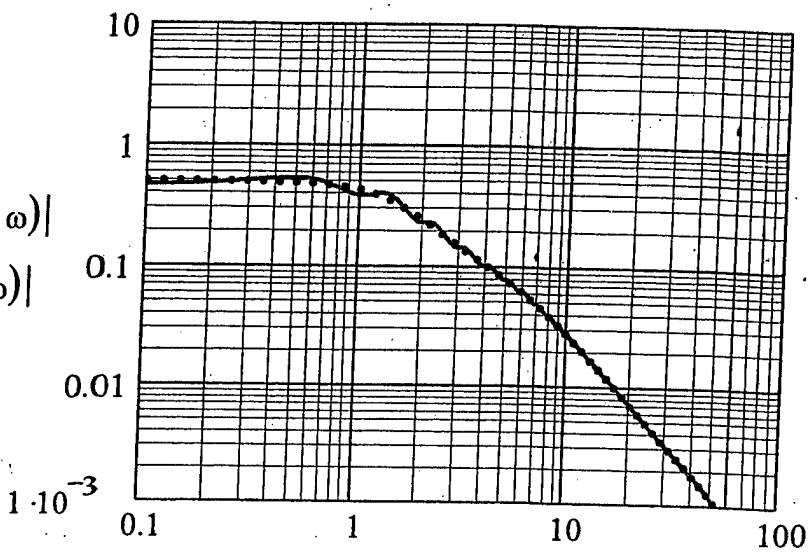

Figure 7.2. The same as Figure 2.2 except that $|R(\omega)|$ is changed from the standard value of [exp(-10^{-3})] to [exp(-2)].

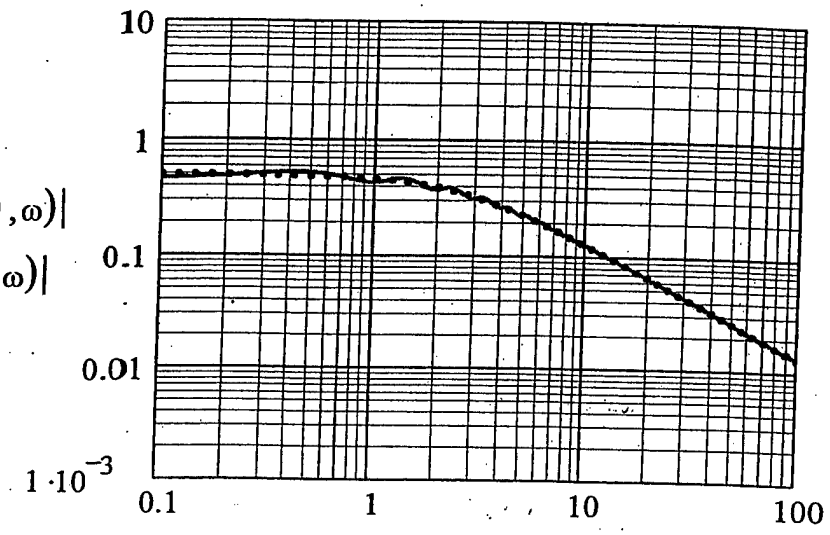

Figure 7.3. The same as Figure 2.3 except that $|R(\omega)|$ is changed from the standard value of [exp(-10^{-3})] to [exp(-2)].

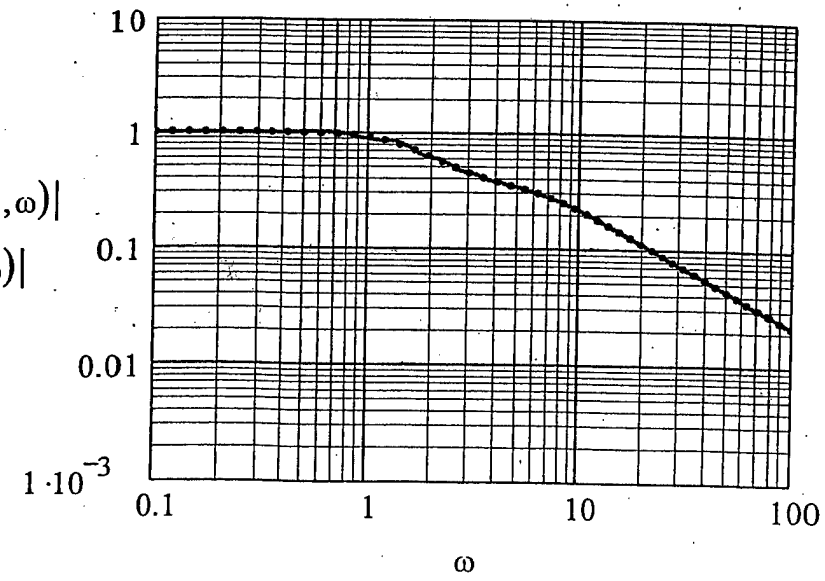

Figure 8.1. The same as Figure 2.1 except that $|R(\omega)|$ is changed from the standard value of [exp(-10^{-3})] to [exp(-π)].

$\frac{|Tbc(k(\omega),\omega)|}{|Tc(k(\omega),\omega)|}$

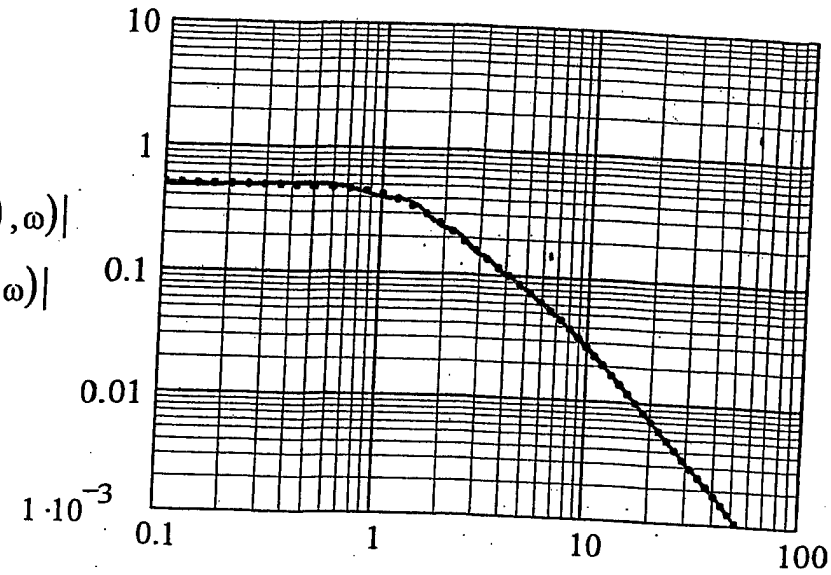

Figure 8.2. The same as Figure 2.2 except that $|R(\omega)|$ is changed from the standard value of [exp(-10^{-3})] to [exp(-π)].

$\frac{|Tb(k(\omega),\omega)|}{|T(k(\omega),\omega)|}$

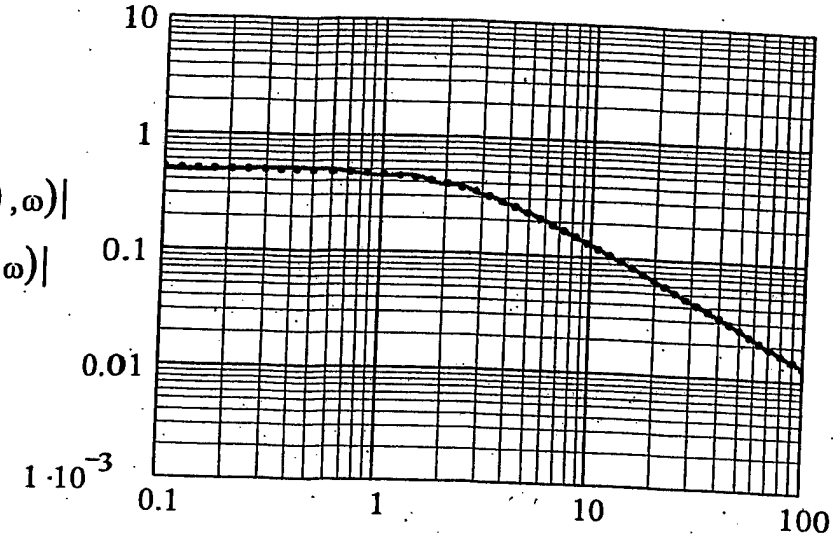

Figure 8.3. The same as Figure 2.3 except that $|R(\omega)|$ is changed from the standard value of [exp(-10^{-3})] to [exp(-π)].

$\frac{|Tbc\_Tb(k(\omega),\omega)|}{|Tc\_T(k(\omega),\omega)|}$

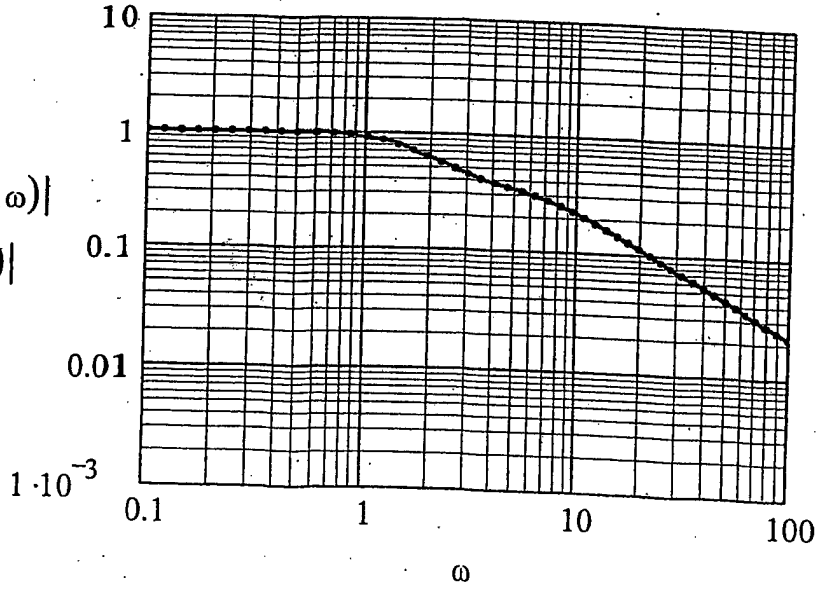

Figure 9.1. The same as Figure 2.1 except that the conditions are augmented by those stated in Equation (21). These augmented conditions are tantamount to rendering $|R(\omega)|$ substantially equal to zero; $|R(\omega)| \Rightarrow 0$.

$$\frac{|Tbc(k(\omega),\omega)|}{|Tc(k(\omega),\omega)|} \quad \bullet\bullet\bullet\bullet\bullet$$

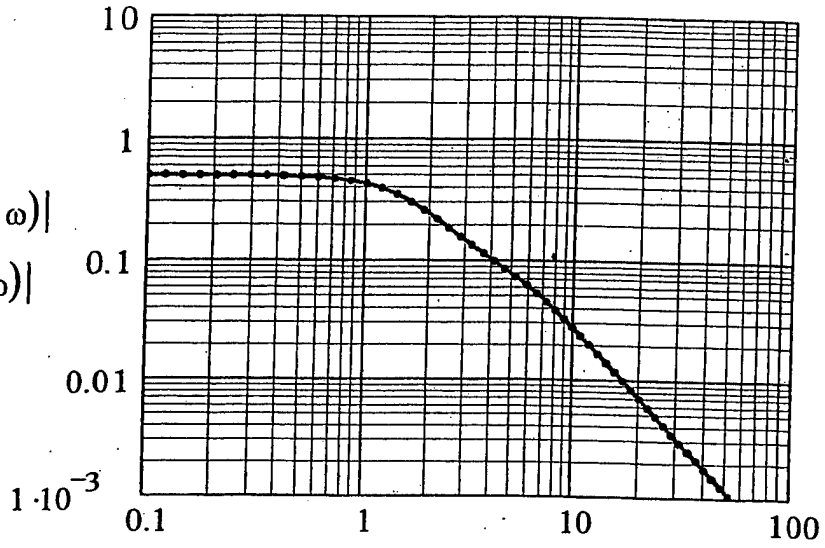

Figure 9.2. The same as Figure 2.2 except that the conditions are augmented by those stated in Equation (21). These augmented conditions are tantamount to rendering $|R(\omega)|$ substantially equal to zero; $|R(\omega)| \Rightarrow 0$.

$$\frac{|Tb(k(\omega),\omega)|}{|T(k(\omega),\omega)|} \quad \bullet\bullet\bullet\bullet\bullet$$

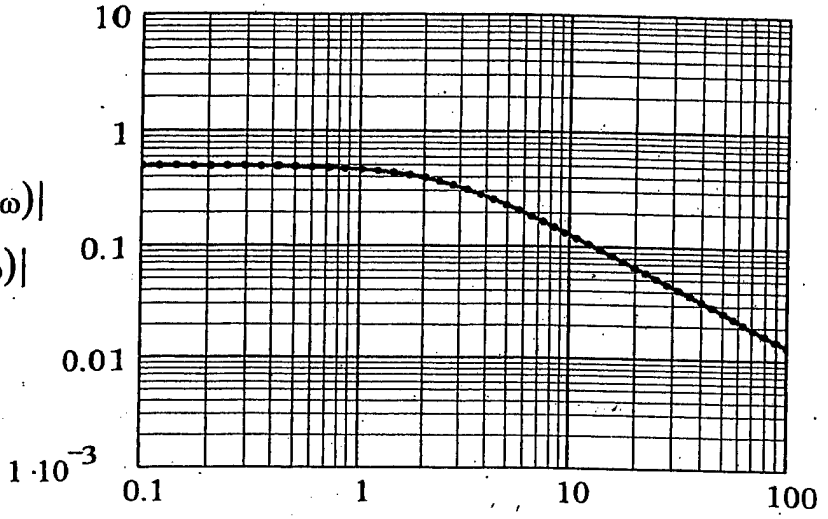

Figure 9.3. The same as Figure 2.3 except that the conditions are augmented by those stated in Equation (21). These augmented conditions are tantamount to rendering $|R(\omega)|$ substantially equal to zero; $|R(\omega)| \Rightarrow 0$.

$$\frac{|Tbc\_Tb(k(\omega),\omega)|}{|Tc\_T(k(\omega),\omega)|} \quad \bullet\bullet\bullet\bullet\bullet$$

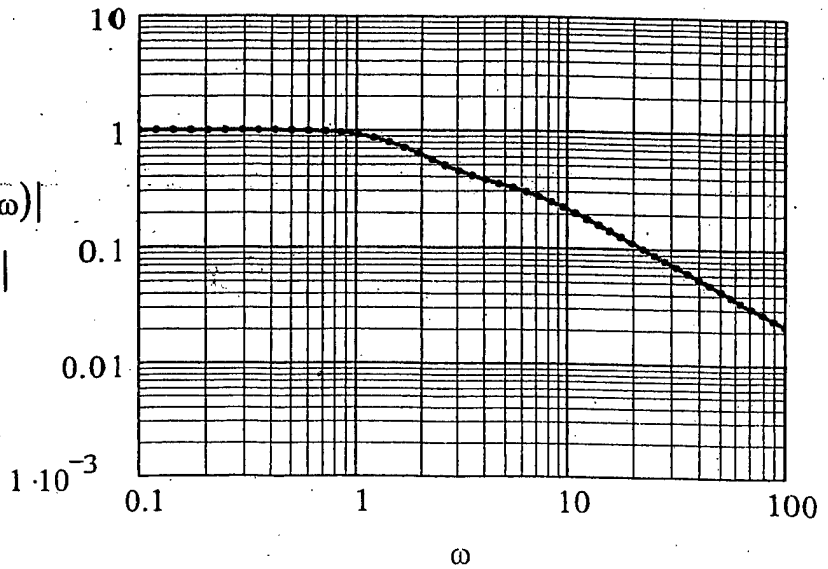

Figure 10.1. The same as Figure 2.1 except that (η) is changed from the standard value of (10^{-2}) to (10^{-4}).

$\frac{|Tbc(k(\omega),\omega)|}{|Tc(k(\omega),\omega)|}$ •••••

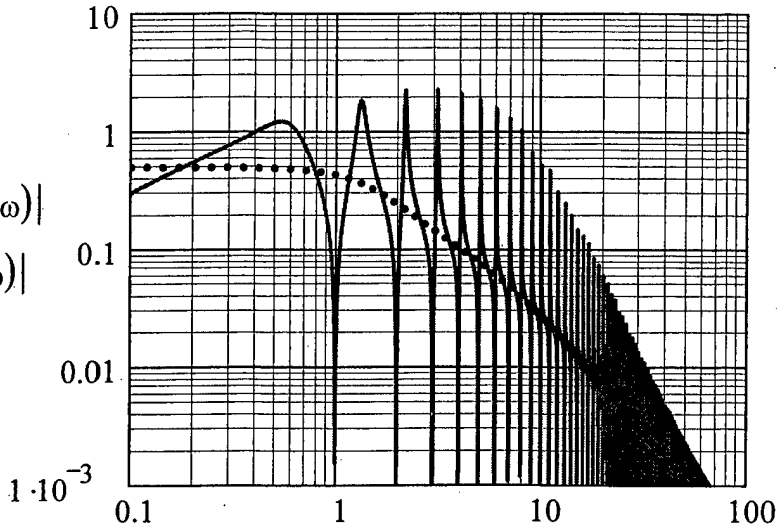

Figure 10.2. The same as Figure 2.2 except that (η) is changed from the standard value of (10^{-2}) to (10^{-4}).

$\frac{|Tb(k(\omega),\omega)|}{|T(k(\omega),\omega)|}$ •••••

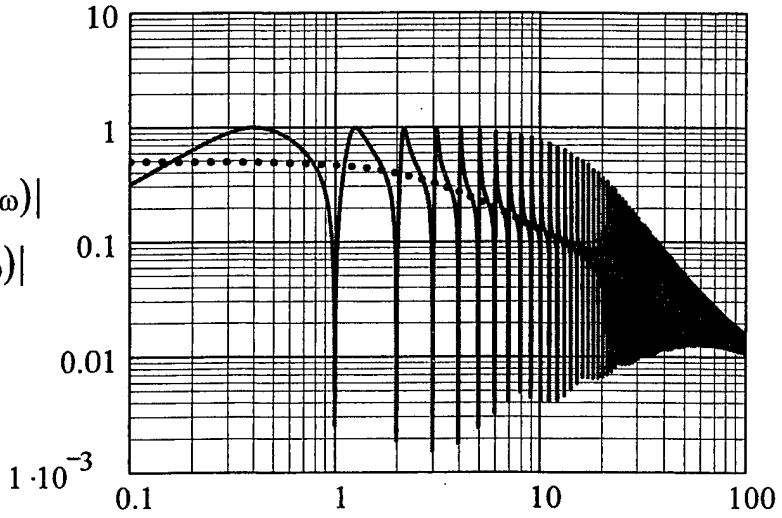

Figure 10.3. The same as Figure 2.3 except that (η) is changed from the standard value of (10^{-2}) to (10^{-4}).

$\frac{|Tbc\_Tb(k(\omega),\omega)|}{|Tc\_T(k(\omega),\omega)|}$ •••••

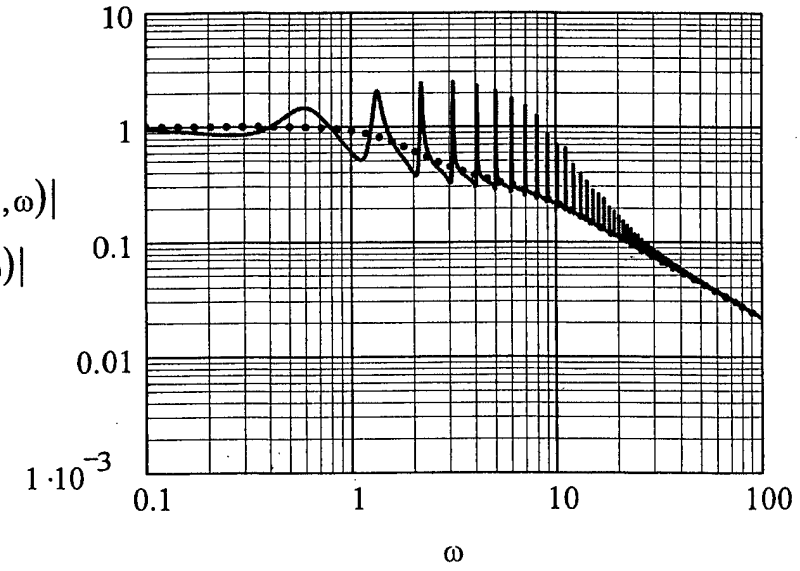

Figure B1.1. The same as Figure 2.1 except that the standard dipole-like external drive with S=1, is changed to monopole-like with S=0.

$\frac{|Tbc(k(\omega),\omega)|}{|Tc(k(\omega),\omega)|}$ .....

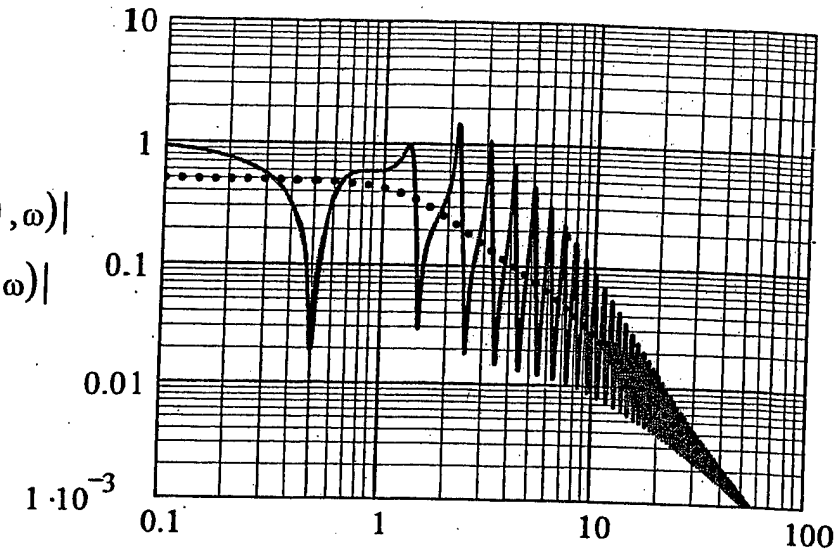

Figure B1.2. The same as Figure 2.2 except that the standard dipole-like external drive with S=1, is changed to monopole-like with S=0.

$\frac{|Tb(k(\omega),\omega)|}{|T(k(\omega),\omega)|}$ .....

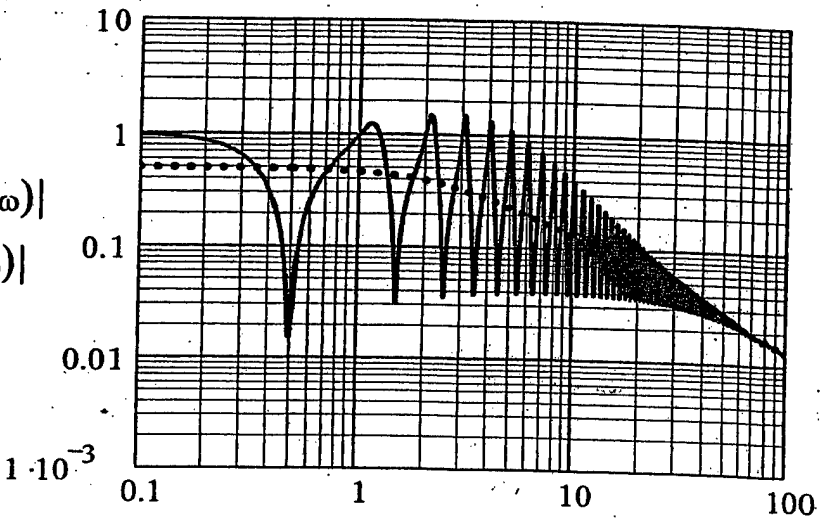

Figure B1.3. The same as Figure 2.3 except that the standard dipole-like external drive with S=1, is changed to monopole-like with S=0.

$\frac{|Tbc\_Tb(k(\omega),\omega)|}{|Tc\_T(k(\omega),\omega)|}$ .....

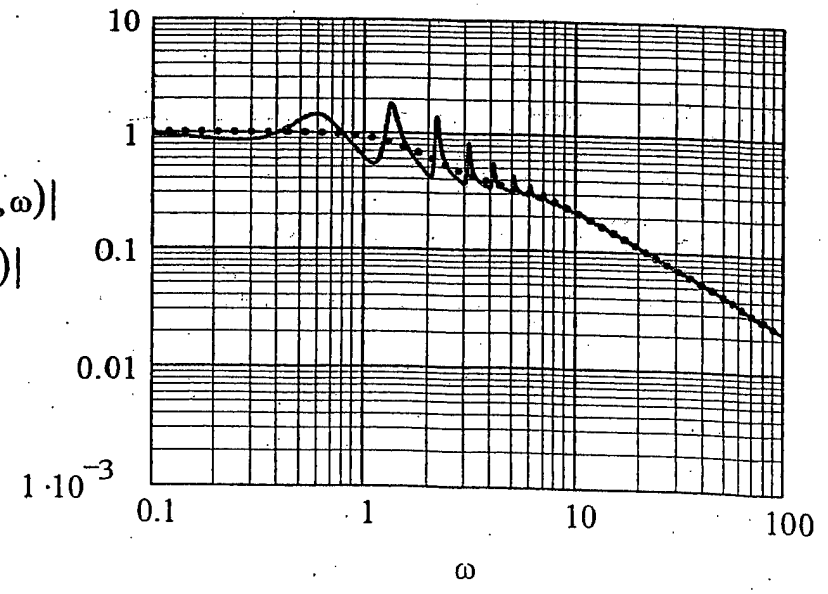

Figure B2.1. The same as Figure 3.1 except that the standard dipole-like external drive with S=1, is changed to monopole-like with S=0. [cf. Figure 2.1.]

$\frac{|Tbc(k(\omega),\omega)|}{|Tc(k(\omega),\omega)|}$ .....

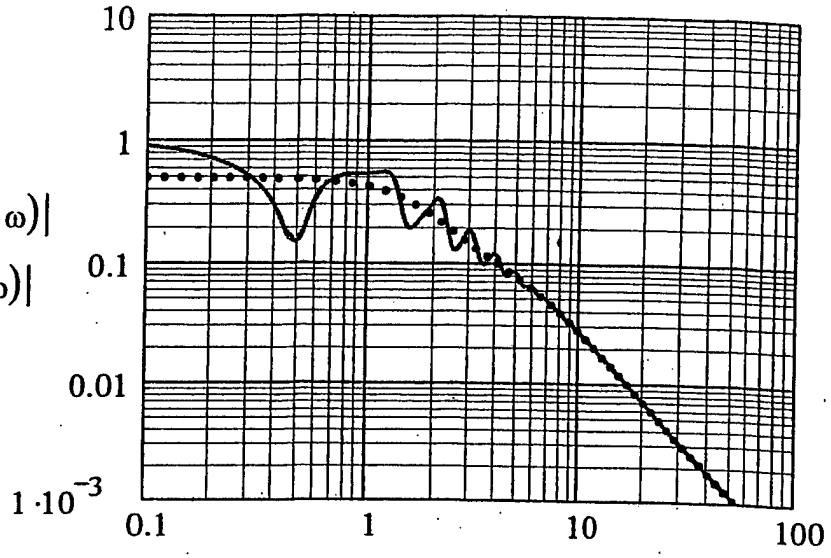

Figure B2.2. The same as Figure 3.2 except that the standard dipole-like external drive with S=1, is changed to monopole-like with S=0. [cf. Figure 2.2.]

$\frac{|Tb(k(\omega),\omega)|}{|T(k(\omega),\omega)|}$ .....

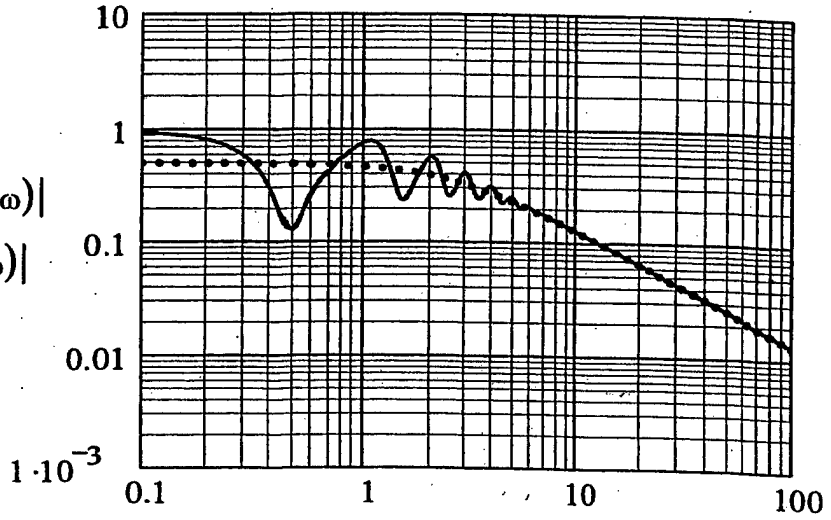

Figure B2.3. The same as Figure 3.3 except that the standard dipole-like external drive with S=1, is changed to monopole-like with S=0. [cf. Figure 2.3.]

$\frac{|Tbc\_Tb(k(\omega),\omega)|}{|Tc\_T(k(\omega),\omega)|}$ .....

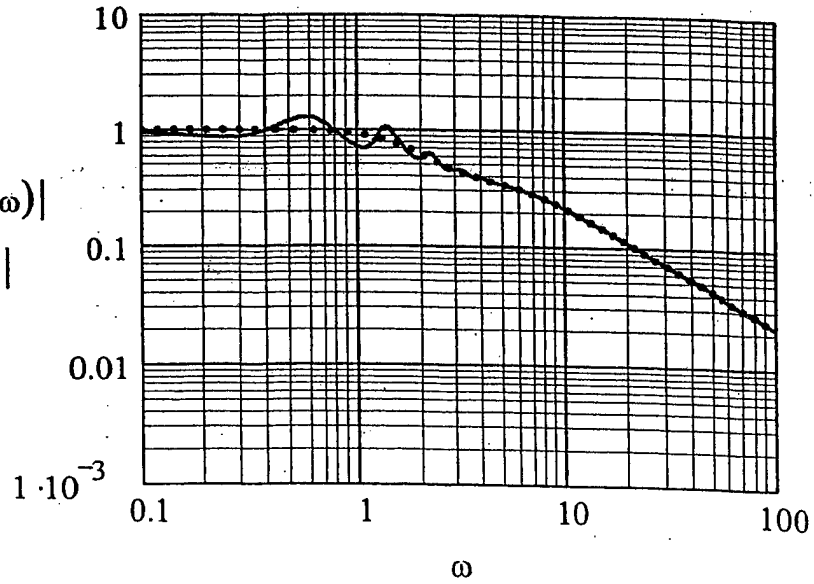

Figure B3.1. The same as Figure 2.1 except that the value of $(b_1 k_o)$ is changed from the standard value of zero to $(b_1 k_o)$= 0.2 (bk_o).

$\frac{|Tbc(k(\omega),\omega)|}{|Tc(k(\omega),\omega)|}$

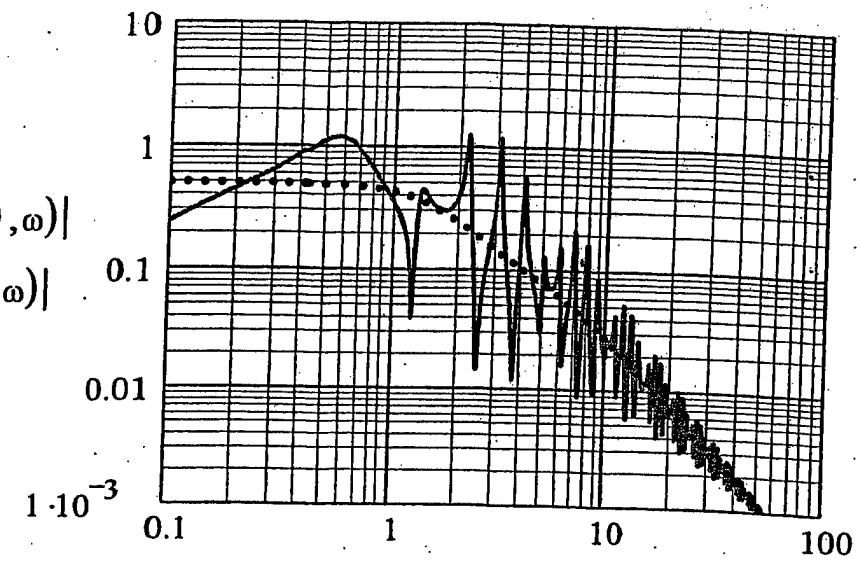

Figure B3.2. The same as Figure 2.2 except that the value of $(b_1 k_o)$ is changed from the standard value of zero to $(b_1 k_o)$= 0.2 (bk_o).

$\frac{|Tb(k(\omega),\omega)|}{|T(k(\omega),\omega)|}$

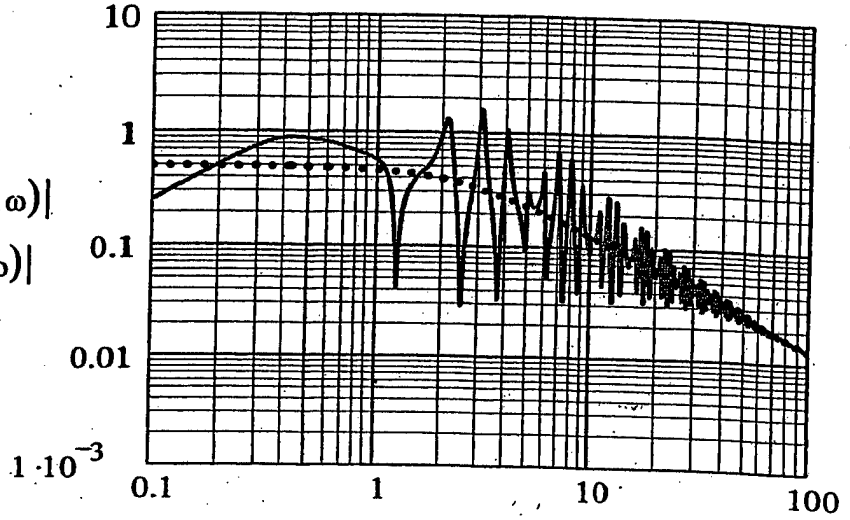

Figure B3.3. The same as Figure 2.3 except that the value of $(b_1 k_o)$ is changed from the standard value of zero to $(b_1 k_o)$= 0.2 (bk_o).

$\frac{|Tbc\_Tb(k(\omega),\omega)|}{|Tc\_T(k(\omega),\omega)|}$

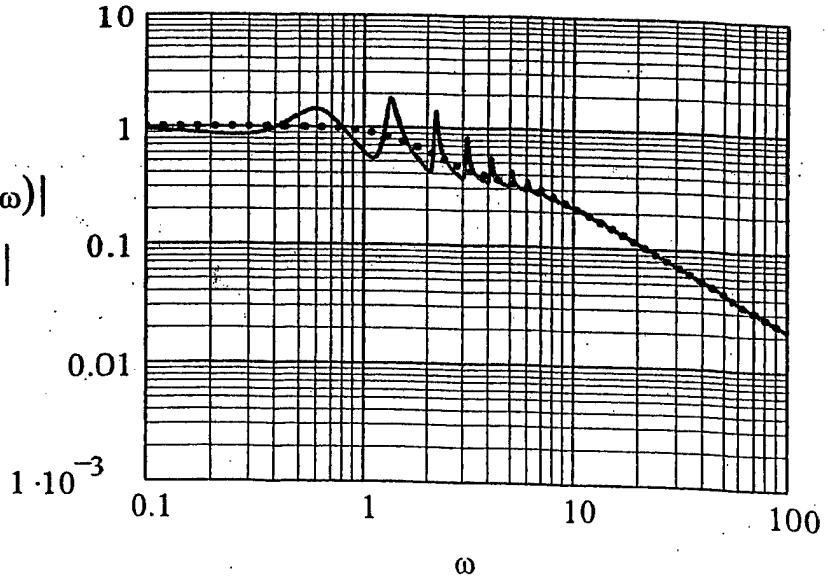

Figure B4.1. The same as Figure 3.1 except that the value of $(b_1 k_o)$ is changed from the standard value of zero to $(b_1 k_o)$= 0.2 $(b k_o)$. [cf. Figure B3.1.]

$\frac{|Tbc(k(\omega),\omega)|}{|Tc(k(\omega),\omega)|}$ •••••

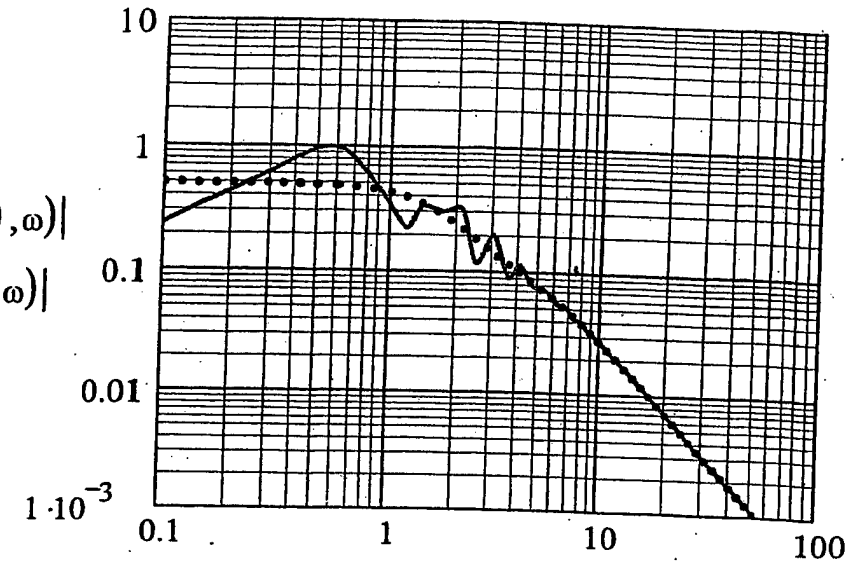

Figure B4.2. The same as Figure 2.2 except that the value of $(b_1 k_o)$ is changed from the standard value of zero to $(b_1 k_o)$= 0.2 $(b k_o)$. [cf. Figure B3.2.]

$\frac{|Tb(k(\omega),\omega)|}{|T(k(\omega),\omega)|}$ •••••

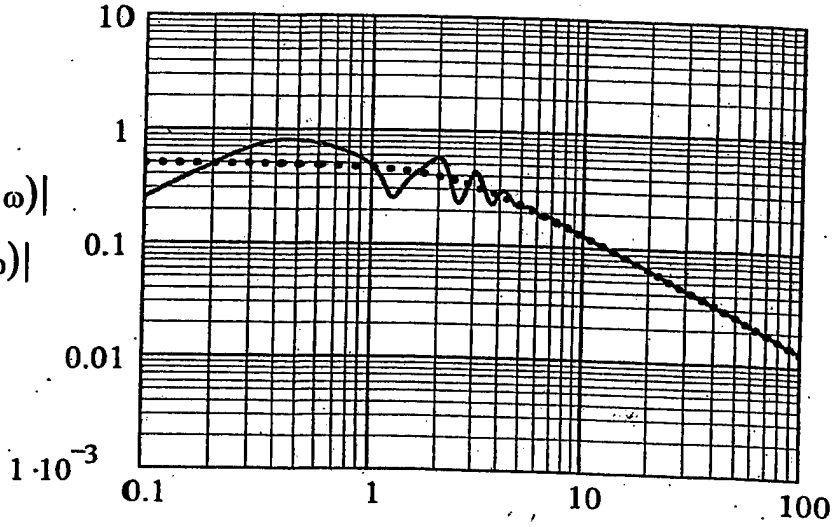

Figure B4.3. The same as Figure 2.3 except that the value of $(b_1 k_o)$ is changed from the standard value of zero to $(b_1 k_o)$= 0.2 $(b k_o)$. [cf. Figure B3.3.]

$\frac{|Tbc\_Tb(k(\omega),\omega)|}{|Tc\_T(k(\omega),\omega)|}$ •••••

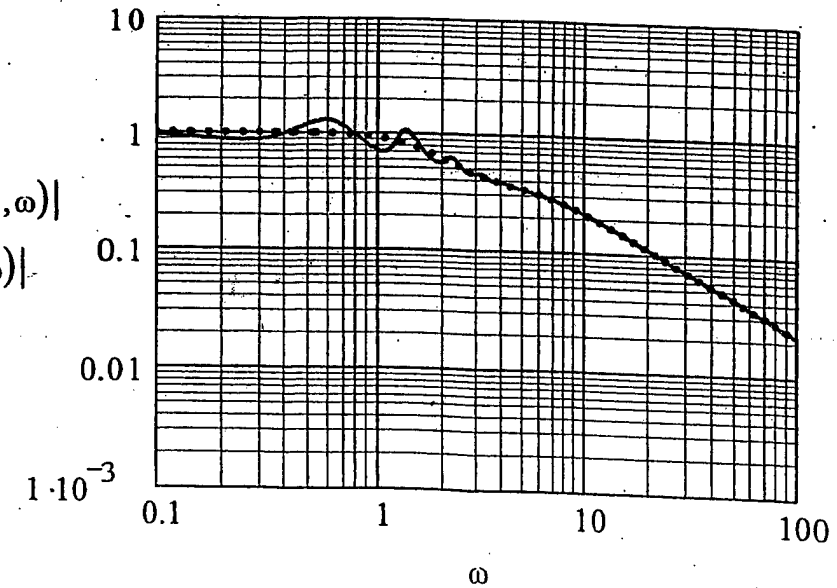

Figure B5.1. The same as Figure 2.1 except that the value of (k/k_o) is changed from the standard value of zero to $(\omega\sqrt{3}/2)$. Note that $k_o = (\omega_o / c_1)$.

$\frac{|Tbc(k(\omega),\omega)|}{|Tc(k(\omega),\omega)|}$ .....

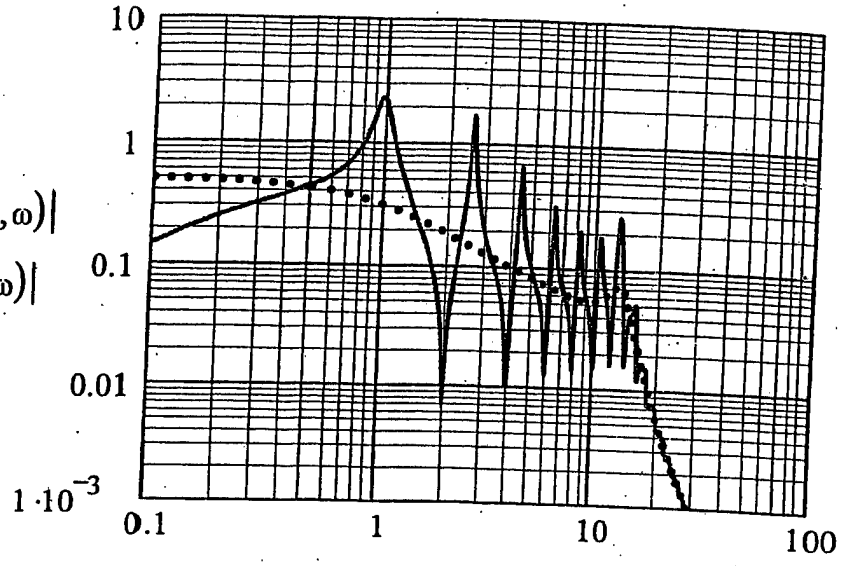

Figure B5.2. The same as Figure 2.2 except that the value of (k/k_o) is changed from the standard value of zero to $(\omega\sqrt{3}/2)$. Note that $k_o = (\omega_o / c_1)$.

$\frac{|Tb(k(\omega),\omega)|}{|T(k(\omega),\omega)|}$ .....

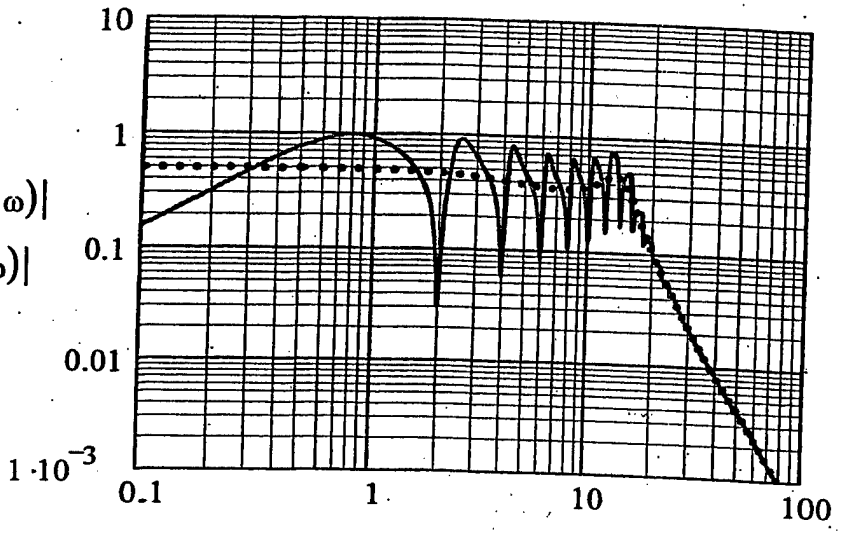

Figure B5.3. The same as Figure 2.3 except that the value of (k/k_o) is changed from the standard value of zero to $(\omega\sqrt{3}/2)$. Note that $k_o = (\omega_o / c_1)$.

$\frac{|Tbc\_Tb(k(\omega),\omega)|}{|Tc\_T(k(\omega),\omega)|}$ .....

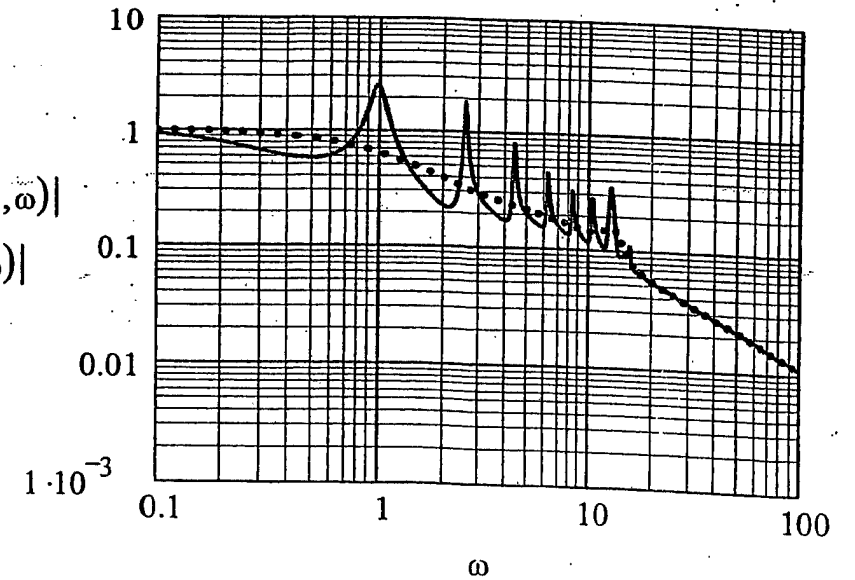

Figure B6.1. The same as Figure 2.1 except that the value of (bk_o) is changed from the standard value of (π) to $(2\pi/\sqrt{\omega})$. [cf. Note that in this figure (bk_o) is made dependent on the normalized frequency.]

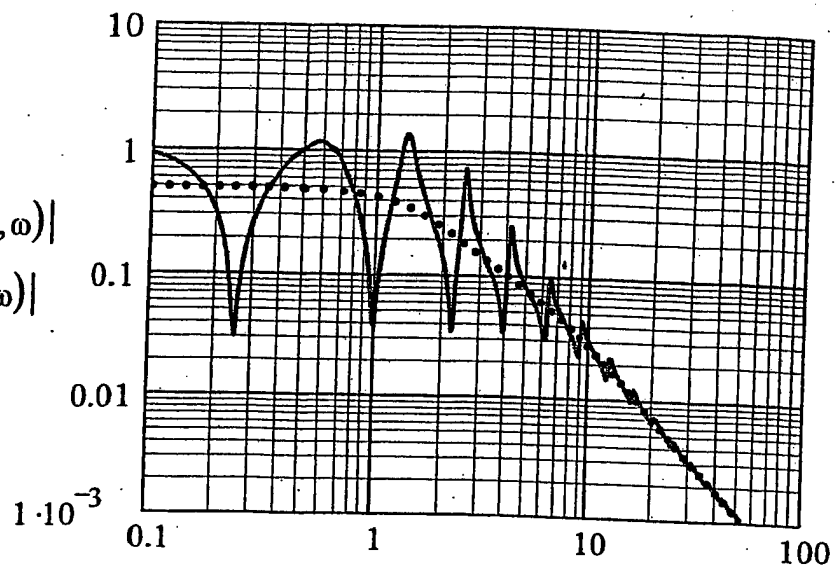

Figure B6.2. The same as Figure 2.2 except that the value of (bk_o) is changed from the standard value of (π) to $(2\pi/\sqrt{\omega})$. [cf. Note that in this figure (bk_o) is made dependent on the normalized frequency.]

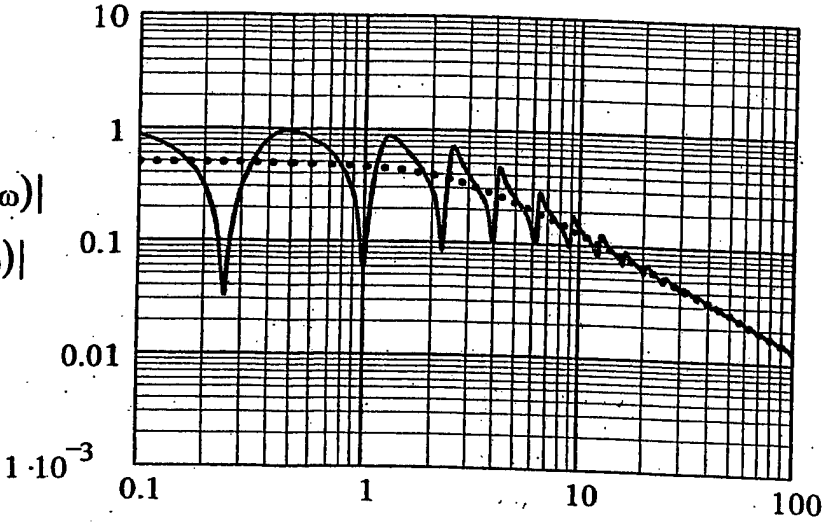

Figure B6.3. The same as Figure 2.3 except that the value of (bk_o) is changed from the standard value of (π) to $(2\pi/\sqrt{\omega})$. [cf. Note that in this figure (bk_o) is made dependent on the normalized frequency.]

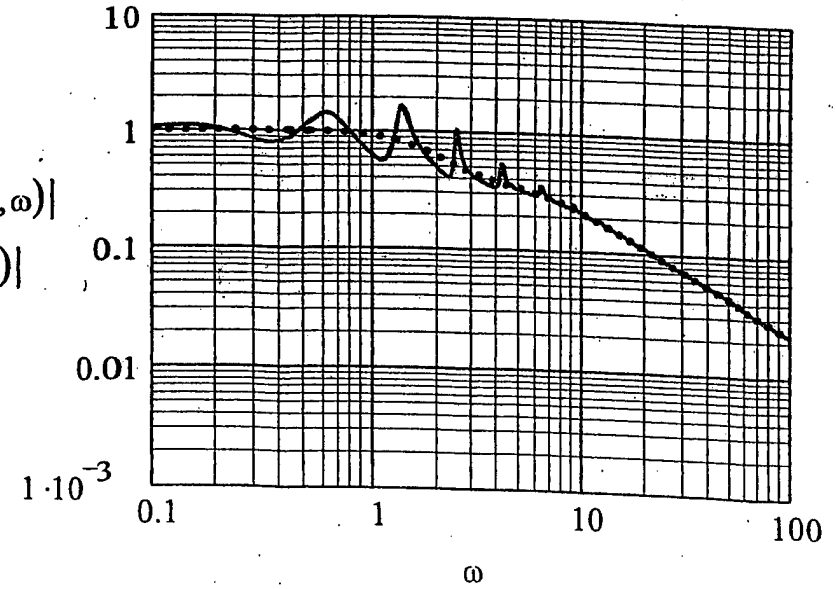

Figure B7.1. The same as Figure 7.1 except that the value of (k/k_o) is changed from the standard value of zero to $(\omega\sqrt{3}/2)$. [cf. Figure B5.]

$$\frac{|Tbc(k(\omega),\omega)|}{|Tc(k(\omega),\omega)|}$$

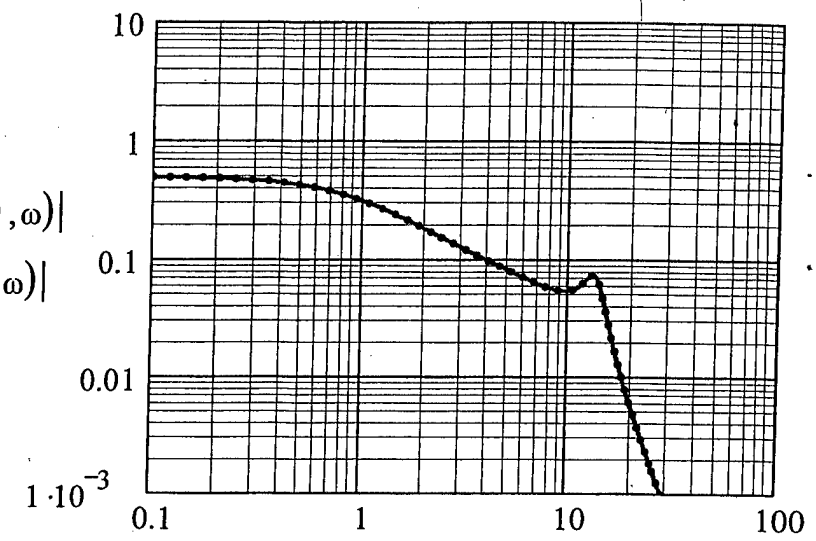

Figure B7.2. The same as Figure 7.2 except that the value of (k/k_o) is changed from the standard value of zero to $(\omega\sqrt{3}/2)$. [cf. Figure B5.]

$$\frac{|Tb(k(\omega),\omega)|}{|T(k(\omega),\omega)|}$$

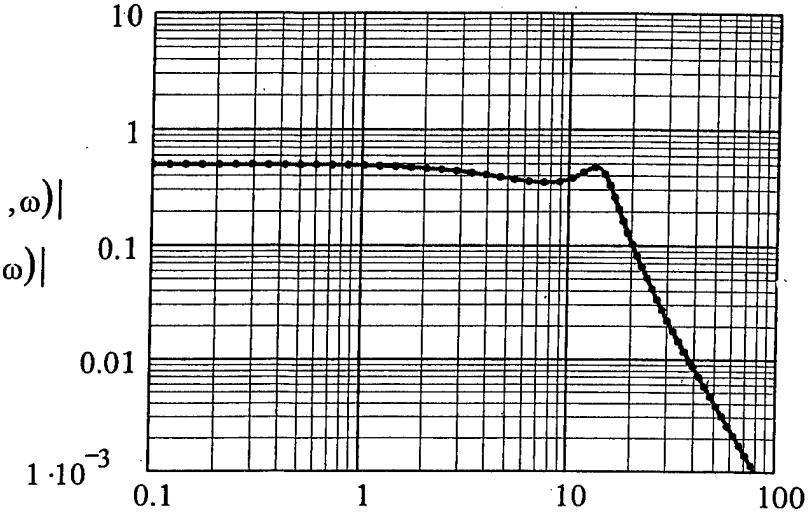

Figure B7.3. The same as Figure 7.3 except that the value of (k/k_o) is changed from the standard value of zero to $(\omega\sqrt{3}/2)$. [cf. Figure B5.]

$$\frac{|Tbc\_Tb(k(\omega),\omega)|}{|Tc\_T(k(\omega),\omega)|}$$

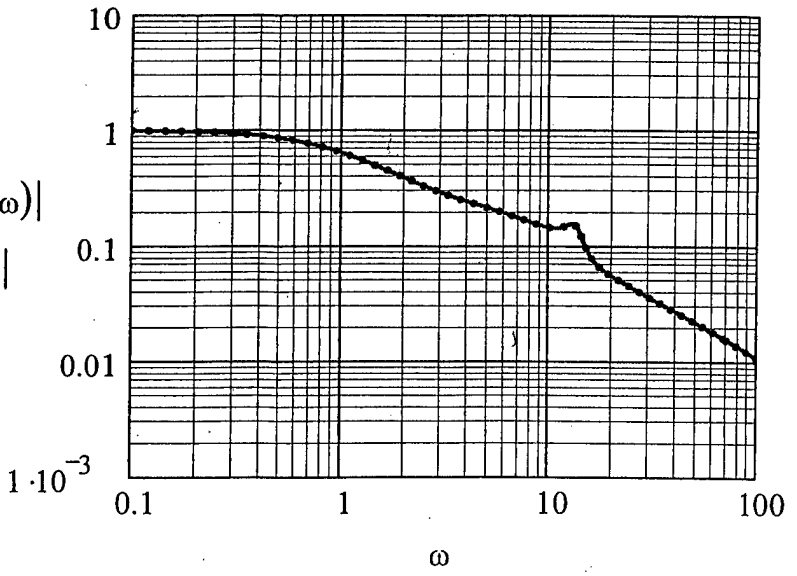

INITIAL DISTRIBUTION

Copies		Copies	Code	Name
3	NAVSEA 05T2	1	7020	Strasberg
	1 Taddeo			
	1 Biancardi	1	7030	Maidanik
	1 Shaw			
		1	7204	Niemiec
3	ONR/ONT			
	1 334 Schreppler	1	7205	Dlubac
	1 334 Couchman			
	1 Library	1	7200	Shang
2	DTIC	3	7250	Noll
				Maga
2	Johns Hopkins University			Diperna
	1 Green			
	1 Dickey	1	3421	TIC-Carderock
4	ARL/Penn State University			
	1 Koopman			
	1 Hwang			
	1 Hambric			
	1 Conlon			
1	R. H. Lyon, Corp.			
	1 Lyon			
1	MIT			
	1 Dyer			
1	Florida Atlantic University			
	1 Venditti			
2	Boston University			
	1 Pierce			
	1 Barbone			
1	University of Michigan			
	1 Vlahopoulos			

CENTER DISTRIBUTION

1	0112	Barkyoumb
1	7000	Jebsen